UNIVERSITY OF CRETE

DEPARTMENT OF MEDICINE

GRADUATE PROGRAMME IN NEUROSCIENCES

SPANISH RESEARCH COUNCIL - UNIVERSIDAD AUTÓNOMA DE MADRID

CENTRO DE BIOLOGIA MOLECULAR SEVERO OCHOA

LABORATORY OF ADULT NEUROGENESIS AND NEURODEGENERATIVE DISEASES

DIPLOMA THESIS

Hilar mossy cells in human patients and a mouse model of Frontotemporal Dementia.

Ο ρόλος των πυλαίων βρυωδών κυττάρων στη μετωποκροταφική άνοια.

Evgenia Kokosali

Diploma Thesis Supervisor: María Llorens-Martín

Heraklion-Madrid

2023

Examination Committee

María Llorens Martín, PhD

Tenured Senior Researcher, Center for Molecular Biology “Severo Ochoa”, Spanish Research Council

Ioannis Charalampopoulos, PhD

Associate Professor of Pharmacology, School of Medicine, University of Crete

Ioannis Zaganas, PhD

Assistant Professor of Neurology, School of Medicine, University of Crete

Acknowledgements

I would like to express my sincere gratitude and appreciation to the following individuals and institutions who have contributed significantly to the completion of this MSc thesis:

First and foremost, I extend my deepest gratitude to my supervisor, Dr María Llorens Martín, for her guidance, invaluable insights, and constant encouragement throughout the research process. Her knowledge and constructive feedback have been instrumental in shaping the direction and quality of this work.

I am indebted to all the members (Carla Rodríguez Moreno, Julia Terreros Roncal, Berenice Márquez Valadez, Elena Moreno Jiménez, Miguel de la Flor García, Marta Gallardo Caballero and Ana Prádanos Senén) of the 'Adult Neurogenesis and Neurodegenerative Diseases' laboratory at CBMSO for their assistance and support throughout the conduction of my thesis.

I am thankful to the members of my examination committee Dr Ioannis Charalampopoulos and Dr Ioannis Zaganas for their scholarly advice, support and willingness to devote their time and insights to this study. I am also grateful to all the faculty members of the Neurosciences Graduate Program of University of Crete, our program's secretary, Jenny Dokoumetzidi and the Department of International and Public Relations staff: Stella Melina Vasilaki and Evi Kortsidaki.

I would like to acknowledge the financial support provided by the Erasmus+ program of the European Commission to University of Crete, as well as, the funding agencies of the laboratory: European Research Council (ERC) (ERC-CoG-2020-101001916), Spain's Ministry of Economy and Competitiveness (PID2020-113007RB-I00, SAF-2017-82185-R and RYC-2015-171899), The Alzheimer's Association (2015-NIRG-340709, AARG-17-528125, and AARG-17-528125-RAPID), The Association for Frontotemporal Degeneration (2016 Basic Science Pilot Grant Award), Center for Networked Biomedical Research on Neurodegenerative Diseases (CIBERNED, Spain), that enabled the successful execution of this research project.

Lastly, I am grateful to my friends and family for their support, patience, and understanding throughout the challenging phases of this journey. Their encouragement and belief in my abilities have been a constant source of motivation and strength.

Curriculum Vitae

EDUCATION

- MSc in Neurosciences, School of Medicine, University of Crete: 09/2021 - Present
- Bachelor's Degree in Biology, Bio-molecular Sciences and Biotechnology domain, Department of Biology, University of Crete: 09/2014-07/2020
- High School Diploma, High School of Nea Alikarnassos: 06/2014

RESEARCH AND WORK EXPERIENCE

- Graduate student: 01/12/2022 – 31/08/2023

  Centro De Biologia Molecular Severo Ochoa, Adult Neurogenesis and Neurodegenerative Diseases Laboratory

  Conduction of MSc thesis: "Hilar Mossy Cells in human patients and a mouse model of Frontotemporal Dementia".

  Supervisor: Dr Llorens Martín María Victoria
- Research Biologist: 01/02/2021 - 31/11/2022

  University of Crete, School of Medicine, Neurology and Neurogenetics Laboratory

  Project title: "Emblematic Action for Neurodegenerative Diseases Research on the Base of Precision Medicine."

  Action title: "Creation of Bank of Biological Material for Neurodegenerative Diseases and their Precursor Forms."

  Scientist responsible for the project: Dr. Mitsias Panagiotis

  Supervisor: Dr Zaganas Ioannis
- Molecular Biologist: 15/01/2022 – 30/09/2022

  Asklipios Diagnosis, Molecular Laboratory

  Detection of SARS-CoV-2 and other viruses for diagnostic purposes.
- Erasmus+ Intern: 02/2020 - 03/2020

  Paris Saclay Institute of Neuroscience, Department of Cognitive Neuroscience, Neurobiology of Decision-Making Team

  Title of internship: "Social behaviour experiments and learning of dedicated software for data analysis."

  Supervisor: Dr Granon Sylvie
- Undergraduate Student: 07/2018 – 09/2019

  University of Crete, School of Medicine, Neurology and Neurogenetics Laboratory

Conduction of BSc thesis: “Localization of TARDBP gene promoter.”
Supervisor: Dr Zaganas Ioannis

- Intern: 06/2018 – 09/2018
  DNA BIOLAB
  Undergraduate practical training in DNAbiolab: research and diagnostic laboratory in Molecular Biology and Genetics.
  Supervisor: Dr Giatzakis Christoforos
- Undergraduate Student: 09/2017 - 03/2018
  University of Crete, Biology Department, Molecular Evolution And Population Genetics Laboratory
  Subject of traineeship: Detection, quantification and statistical analysis of heteroplasmy in Drosophila mauritiana and Drosophila simulans strains.
  Supervisor: Dr Ladoukakis Emmanuel

LANGUAGES

Greek: Native

English: C2

French: B2

SCHOLARSHIPS

- Erasmus+ Graduate Scholarship, University of Crete, December 2022
- Erasmus+ Undergraduate Scholarship, University of Crete, Athens University of Economics and Business, March 2020
- Chrisanthos And Anastasia Karidis Excellence Scholarship, University of Crete, March 2016

PUBLICATIONS

1. Twist exome capture allows for lower average sequence coverage in clinical exome sequencing.
   Yaldiz, B., Kucuk, E., Hampstead, J., Hofste, T., Pfundt, R., Corominas Galbany, J., Rinne, T., Yntema, H. G., Hoischen, A., Nelen, M., Gilissen, C., Solve-RD consortium “Human Genomics”, May 2023, DOI: 10.1186/s40246-023-00485-5

2. A Solve-RD ClinVar-based reanalysis of 1522 index cases from ERN-ITHACA reveals common pitfalls and misinterpretations in exome sequencing.
   Denommé-Pichon, A. S., Matalonga, L., de Boer, E., Jackson, A., Benetti, E., Banka, S., Bruel, A. L., Ciolfi, A., Clayton-Smith, J., Dallapiccola, B., Duffourd, Y., Ellwanger, K., Fallerini, C., Gilissen, C., Graessner, H., Haack, T. B., Havlovicova, M., Hoischen, A., Jean-Marçais, N., Kleefstra, T., …, Faivre, L.
   "Genetics in Medicine", April 2023, DOI: 10.1016/j.gim.2023.100018
3. Study of Alzheimer's disease and Frontotemporal dementia- associated genes in the Cretan Aging Cohort.
   Mathioudakis, L., Dimovasili, C., Bourbouli, M., Latsoudis, H., Kokosali, E., Gouna, G., Vogiatzi, E., Basta, M., Kapetanaki, S., Panagiotakis, S., Kanterakis, A., Boumpas, D., Lionis, C., Plaitakis, A., Simos, P., Vgontzas, A., Kafetzopoulos, D., Zaganas, I.
   "Neurobiology of Aging", 2022, DOI: 10.1016/j.neurobiolaging.2022.07.002
4. The association of basal cortisol levels with episodic memory in older adults is mediated by executive function.
   Antypa, D., Basta, M., Vgontzas, A., Zaganas, I., Panagiotakis, S., Vogiatzi, E., Kokosali, E., Simos, P
   "Neurobiology of Learning and Memory", 2022, DOI: 10.1016/j.nlm.2022.107600

PRESENTATIONS/ABSTRACTS SUBMITTED TO CONFERENCES

1. CADASIL syndrome in a family with vascular encephalopathy caused by a newly described mutation in the NOTCH3 gene.
   Tsiverdis, Kokosali*, Skoula, Zafeiris, Mitsias, Zaganas
   Oral presentation for the 33rd Hellenic Meeting for Neurology, 2022
2. Patient with adult-onset leukodystrophy caused by two mutations in the AARS gene.
   Kovas*, Marogianni, Kokosali, Tsiverdis, Zaganas, Papadimitriou
   Oral presentation for the 33rd Hellenic Meeting for Neurology, 2022
3. Whole Exome Sequencing yield across heterogeneous neurologic phenotypes.
   Kokosali, Tsiverdis*, Mathioudakis, Spilioti, Skoula, Evangeliou, Zaganas
   Abstract for the European Academy of Neurology Congress, 2022
4. Treatable myopathies, detected with Next Generation Sequencing methods.
   Tsiverdis*, Mathioudakis, Latsoudi, Kotzamani, Skoula, Kokosali, Bitsori, Vergadi, Vorgia, Galanakis, Evangeliou, Zaganas
   Abstract for the 32nd Hellenic Meeting for Neurology, 2021

Abstract

Frontotemporal Dementia (FTD) is a neurodegenerative disorder that involves the progressive degeneration of the frontal and temporal lobes, with the patients displaying behavioural or language symptoms. Frontotemporal Dementia and Parkinsonism linked to chromosome 17 (FTDP-17) is a subtype of FTD that falls into the category of tauopathies. Mutations in the MAPT gene are associated with this disorder. Hilar Mossy Cells (MCs), a glutamatergic subtype of neurons of the dentate gyrus (DG), are implicated in several pathological conditions like Temporal Lobe Epilepsy (TLE), Schizophrenia (SCZ) and Alzheimer's Disease (AD). In this project, we studied the changes in MCs in a transgenic mouse model of FTDP-17 (Tau^{VLW}), harbouring mutations in the MAPT gene, and in human patients of FTD. We found that, compared to control mice, Tau^{VLW} mice show a decreased volume of both the dorsal and ventral DG, and a decrease in the number of MCs in the ventral DG. We also showed that the expression of Calretinin (CR), which is considered a gold-standard marker for MCs, follows a latero-medial gradient in the dorsal DG. In patients with FTD, the density of CR^+ MCs showed no changes compared to healthy control subjects; however, we found a decrease in the densities of CR^+ immature dentate granule cells (DGCs) and CR^+ interneurons. By performing qualitative determinations, we showed that distinct subpopulations of MCs, expressing different molecular markers, are present in the human DG. Together, these data suggest that MCs are vulnerable to neurodegeneration mechanisms present in mouse models and patients with FTD. Further investigation is needed to shed light on the underlying mechanisms behind MC loss and/or dysfunction.

Keywords: Hilar Mossy Cells (MCs), Frontotemporal Dementia and Parkinsonism linked to chromosome 17 (FTDP-17), MAPT, Tauopathies, Calretinin (CR), Dysbindin-1C

Περίληψη

Η μετωποκροταφική άνοια (FTD) είναι μια νευροεκφυλιστική διαταραχή που χαρακτηρίζεται από τον προοδευτικό εκφυλισμό του μετωπιαίου και κροταφικού λοβού, με τους ασθενείς να εμφανίζουν συμπεριφορικά ή γλωσσικά συμπτώματα. Η μετωποκροταφική άνοια και ο παρκινσονισμός που συνδέονται με το χρωμόσωμα 17 (FTDP-17) είναι ένας υποτύπος FTD που εμπίπτει στην κατηγορία των ταυοπαθειών. Μεταλλάξεις στο γονίδιο MAPT έχουν συσχετιστεί με αυτή τη διαταραχή. Τα βρυώδη κύτταρα (MCs), ένας γλουταμινεργικός υπότυπος νευρώνων της οδοντωτής έλικας (DG), εμπλέκονται σε διάφορες παθολογικές καταστάσεις όπως η επιληψία του κροταφικού λοβού (TLE), η σχιζοφρένεια (SCZ) και η νόσος Alzheimer (AD). Σε αυτή την εργασία, μελετήσαμε τις αλλαγές των MCs σε ένα διαγονιδιακό μοντέλο ποντικού FTDP-17 (Tau^{VLW}), που φέρει μεταλλάξεις στο γονίδιο MAPT και σε ανθρώπους που έπασχαν από FTD. Βρήκαμε ότι, σε σύγκριση με τα ποντίκια ελέγχου, τα ποντίκια Tau^{VLW} εμφανίζουν μειωμένο όγκο τόσο της ραχιαίας όσο και της κοιλιακής DG και μια μείωση στον αριθμό των MCs στην κοιλιακή DG. Δείξαμε επίσης ότι η έκφραση της καλρετινίνης (CR), η οποία θεωρείται ο πιο τυπικός δείκτης των MCs, ακολουθεί μια κλίση στον μεσοπλευρικό άξονα στη ραχιαία DG. Σε ασθενείς με FTD, η πυκνότητα των CR^+ MCs δεν έδειξε αλλαγές σε σύγκριση με υγιή άτομα. Ωστόσο, βρήκαμε μείωση στις πυκνότητες των CR^+ ανώριμων κοκκοειδών κυττάρων της DG (DGCs) και CR^+ ενδονευρώνων. Εκτελώντας ποιοτικούς προσδιορισμούς, δείξαμε ότι διακριτοί υποπληθυσμοί MCs, που εκφράζουν διαφορετικούς μοριακούς δείκτες, υπάρχουν στην ανθρώπινη DG. Μαζί, αυτά τα δεδομένα υποδηλώνουν ότι τα MCs είναι ευάλωτα στην νευροεκφύλιση που παρατηρείται σε μοντέλα ποντικών και ασθενείς με FTD. Απαιτείται περαιτέρω έρευνα για να ρίξει φως στους υποκείμενους μηχανισμούς πίσω από την απώλεια και/ή τη δυσλειτουργία των MCs.

Λέξεις-κλειδιά: Βρυώδη κύτταρα (MCs), Μετωποκροταφική άνοια με Παρκινσονισμό που συνδέεται με το χρωμόσωμα 17 (FTDP-17), MAPT, Ταυοπάθειες, Καλρετινίνη (CR), Δυσμπινδίνη-1C

Contents

Abbreviations

Aβ: Amyloid Beta

AD: Alzheimer's Disease

AD: Alzheimer's disease

AHN: Adult Hippocampal Neurogenesis

BV-FTD: Behavioural variant FTD

CA1, CA2, CA3/CA4: Cornu Ammonis regions in the hippocampal formation

CBD: Corticobasal degeneration

CA1, CA2, CA3/CA4: Cornu Ammonis regions in the hippocampal formation

C9orf72: Chromosome 9 Open Reading Frame 72

CBD: Corticobasal degeneration

CHMP2B: Chromatin modifying protein 2B

CIEN: Centro de Investigación de Enfermedades Neurológicas

CNS: Central Nervous System

CR: Calretinin

D2R: Dopamine D2 receptor

DA: Dopamine

DAPI: 4',6-diamidino-2-phenylindole

DG: Dentate Gyrus

EPSP: Excitatory Postsynaptic Potential

EC: Entorhinal Cortex

FDA: U.S. Food and Drug Administration

FTD: Frontotemporal dementia

FTD-Tau: Frontotemporal dementia with Tau pathology

FTDP: Frontotemporal dementia with parkinsonism

FTLD: Frontotemporal lobar degeneration

FTLD-TDP: Frontotemporal lobar degeneration with TDP-43 pathology

FTLD-Tau: Frontotemporal lobar degeneration with Tau pathology

GCL: Granule Cell Layer

GRN: Progranulin

IHC: Immunohistochemistry

LV-PPA: Logopenic variant PPA

MAPT: Microtubule-associated protein tau

MC(s): Mossy Cell(s)

ML: Molecular Layer

NMDA: N-Methyl-D-Aspartate

NFV-PPA: Non-fluent variant primary progressive aphasia

NSC: Neural Stem Cell

PB: Phosphate buffer

PBS: Phosphate buffered saline

PFA: Paraformaldehyde

PSA-NCAM: Polysialylated-neural cell adhesion molecule

PSP: Progressive supranuclear palsy

SCZ: Schizophrenia

Shh: Sonic Hedgehog

SE: Status Epilepticus

SSRIs: Selective serotonin reuptake inhibitors

SV-PPA: Semantic variant PPA

TDP-43: TAR DNA binding protein 43

TLE: Temporal Lobe Epilepsy

UBQLN2: Ubiquilin-2

VCP: Valosin-containing protein

WT: Wild Type

Introduction

Frontotemporal Dementia

Frontotemporal dementia (FTD) is a general clinical term that includes several gradual neurodegenerative clinical patterns characterized by progressive impairments in behaviour, executive function and language. This form of dementia is frequent among individuals under the age of 65 years old and can often resemble different psychiatric conditions due to its typical behavioural symptoms. One of the most remarkable features of FTD is the degeneration of the frontal and anterior temporal lobes.

Clinical Manifestations

As mentioned above, the term FTD is an umbrella term that includes different disease subtypes. The main clinical variants of FTD are the behavioural-variant FTD (BV-FTD), which displays early impairments in behaviour and executive function; the non-fluent variant primary progressive aphasia (NFV-PPA), characterized by gradual language deficits involving speech, grammar and word expression; the semantic-variant PPA (SV-PPA), a progressive condition affecting semantic knowledge and naming abilities; and the logopenic PPA (LV-PPA), which manifests with errors in word retrieval and sentence repetition.[1,2] As the disease advances, the symptoms of the distinct variants can converge, as the initial localized degeneration diffuses and affects more areas in the frontal and temporal lobes. With the passage of time, the patients suffer from general cognitive decline and motor issues, which may include parkinsonism.[2] Parkinsonism occurs in 20% of FTD patients and is most usually observed in patients with BV-FTD, followed by patients with NFV-PPA.[3] There is also a notable overlap of clinical symptoms between FTD andother neurodegenerative disorders, like motor neuron disease accompanied with FTD symptoms (FTD-MND), progressive supranuclear palsy (PSP) and corticobasal degeneration (CBD).[1] In the advanced stages of the disorder, individuals struggle with movement, eating and swallowing deficits. Typically, about 8 years following symptom onset, patients succumb to the disease, usually due to secondary infections (i.e. pneumonia).[2]

Epidemiology

FTD ranks as the third most prevalent dementia type across all age groups, after Alzheimer's disease (AD) and dementia with Lewy bodies, and is the leading type of early-onset dementia (<65 years).[1,4] The prevalence of FTD is estimated at 15–22 people per 100,000, and its incidence at 2.7–4.1/100,000.[5] Variations in prevalence are observed in different geographical regions. For instance, within the US population, FTD was found to affect 15 to 22 individuals per 100,000, while in the UK, the numbers ranged from 3 to 26 per 100,000.[6–8] In USA and Europe, the most prevalent FTD subtype is BV-FTD, whereas in Asia, SV-PPA or BV-FTD are the most common variants of the disorder.[6,8] The majority of individuals (60%) with this condition experience disease onset between the ages of 45 and 64. However, a subset of patients (10%) can exhibit initial symptoms of FTD before the age of 45, while 30% of

patients experience symptoms after turning 64.[6] It should be noted that most of the studies published until now concern Europe and the US, leading to underrepresentation of non-Caucasian populations. Also, due to the under-recognition and misdiagnosis of the disorder, the reported prevalence numbers are likely lower than the actual occurrence rate. The survival time after the onset of the symptoms can vary between 6-11 years, depending on the subtype of the disease.[2] In most patients the clinical diagnosis is achieved a few years after the symptom onset, so the survival period from the time of the diagnosis is significantly shorter. The best prognosis concerns the patients affected by the SV-FTD (survival time: >5 years), followed by the NFV-PPA (survival time: 5 years) and the BV-FTD (survival time: 3-4 years), while patients with the MND-FTD have the shortest time of survival since the time of diagnosis (2 years).[2,6,7]

Molecular Pathophysiology

Macroscopic changes in FTD include atrophy in specific brain areas. The atrophy begins in the frontal cortex and hippocampus (stage 1). In stage 2, the atrophy affects additional areas such as the orbitofrontal gyrus, basal ganglia, and posterior temporal lobe. Subsequent stages involve more pronounced frontal and temporal atrophy along with the involvement of white matter (stage 3). Finally, in stage 4, there is severe atrophy in various regions including frontotemporal areas, hippocampus, basal ganglia, and thalamus. These stages align with the severity of dementia and how long the disease has been present.[9,10]

Microscopic changes associated with FTD include neural cell death, enlarged neurons, synaptic loss, loss of myelin in white matter, microvacuolar alterations and gliosis.[11] These modifications are observed in the anterior cingulate cortex, orbitofrontal cortex, fronto-insular cortex and cingulate-frontal transitional zones. Layer 5 of these areas contains von Economo neurons and fork cells, which are believed to be important for integrating cortical and subcortical networks responsible for language and behavioral regulation. These cells degenerate very early in BV-FTD.[12] FTLD, as several other neurodegenerative diseases, typically involves the buildup of protein aggregates or inclusions inside neurons and glial cells. Those characteristic patterns of abnormal protein accumulation are used to define different pathological subtypes of the disease, i.e. if the aggregates consist of microtubule-associated protein tau (MAPT) the subtype is referred to as FTLD-tau, for transactive response DNA-binding protein 43 kDa (TDP-43) aggregates it is FTLD-TDP or if the aggregates are of fused-in-sarcoma (FUS) protein, we have FTLD-FUS.[13] Patients with inclusion of those three proteins account for nearly all cases of FTLD, with FTLD-tau and FTLD-TDP constituting the majority (about 90%).[14,15] A very small number of FTD patients have inclusions that only have ubiquitin or p62, or no inclusions at all.[16]

Genetics

Approximately 20% of FTD cases stem from genetic mutations, while 40% of FTD patients exhibit a familial history of dementia, psychiatric conditions, or motor symptoms, while not displaying a clear

inheritance pattern.[17,18] Genetic FTD patients display diverse symptoms that are observed in all the conditions of the FTD spectrum.[9] The majority of these conditions follow an autosomal dominant inheritance pattern.[19] The most commonly identified genes with mutations linked to FTD are MAPT, Chromosome 9 Open Reading Frame 72 (C9orf72), TAR DNA binding protein (TARDBP), FUS, Progranulin (GRN), Valosin-containing protein (VCP), chromatin modifying protein 2B (CHMP2B), and Ubiquilin-2 (UBQLN2).[19] The penetrance of the disease varies depending on the underlying genetic alteration. Among all the FTD clinical subtypes, FTD-ALS has the highest heritability.[19] FTD with parkinsonism (FTDP) is one of the most significant degenerative dementia syndromes, especially in cases where patients encounter cognitive, behavioural, or motor problems earlier in life (before the age of 65).[20] Most cases of FTDP-17 show the presence of filaments consisted of hyperphosphorylated tau protein and more than 50 mutations in the MAPT gene have been found in different families with FTDP, with this subtype of the disease being labelled as FTDP linked to chromosome 17 (FTDP-17).[21] Taking this into consideration, along with the fact that Tau protein accumulation is also involved in other neurodegenerative diseases (i.e. AD), for this project we used a transgenic mouse model of FTDP-17, which harbours mutations in the MAPT gene.

Tau Protein - Frontotemporal Dementia and Parkinsonism linked to chromosome 17

The MAPT gene is located on chromosome 17q21. In the human brain, the MAPT gene produces six different tau isoforms via alternative mRNA splicing.[22,23] This generates a variety of isoforms with different numbers of microtubule-binding repeats (*Figure 1*). Specifically, alternative splicing of exon 10 results in the production of these six isoforms: three isoforms containing three microtubule-binding repeats each (referred to as 3R) and three isoforms containing four microtubule-binding repeats each (referred to as 4R).[22,23] These repeats are located toward the carboxy terminal of the protein. In the amino terminus, each isoform includes insertions of either 29 or 58 amino acids, or no insert.[22,23] This is why there are three different isoforms with 3R and three different isoforms with 4R, that are referred to as 1N, 2N, and 0N forms.[22,23] During brain development, the 3R tau isoform is more prevalent. However, in the adult human brain, the levels of 3R and 4R tau are approximately equal. Maintaining a proper balance between these 3R and 4R tau isoforms is crucial for preventing early neurodegeneration in the human brain.[23] When tau aggregates in neurons and/or glia, various pathologies can occur that are referred to as tauopathies. Tauopathies include Alzheimer's disease (AD), PSP, CBD, Pick's disease, chronic traumatic encephalopathy (CTE), and frontotemporal dementia with parkinsonism linked to chromosome 17 (FTDP-17).[24]

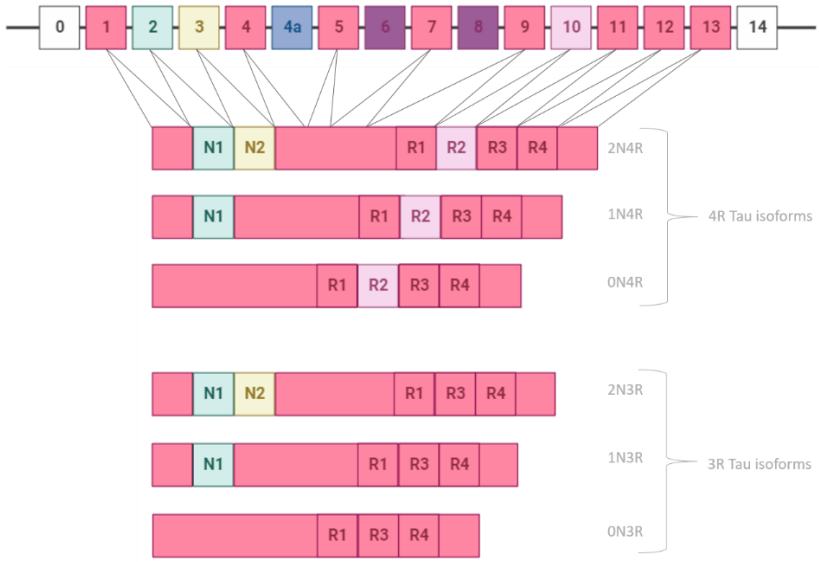

Figure 1: MAPT gene and human Tau isoforms. Top: MAPT gene exons. Bottom: 6 Tau isoforms in the human CNS. Figure created with Biorender.

FTD-associated mutations in the MAPT gene tend to exhibit high penetrance. Almost all FTD-Tau patients have a family history of dementia or parkinsonism.[17] The onset of symptoms for those patients varies between the ages of 20 and 80 years old, with an average onset in the 5th decade of life.[9] The symptoms that characterize FTDP-17 are behavioral and personality disturbances, cognitive deficits and motor dysfunction (usually parkinsonism-plus syndrome).[25] Often, there is a prolonged period of psychiatric symptoms (in some cases schizophrenic-like) preceding the diagnosis.[26] Among patients with mutations in the same gene or patients of the same family, clinical presentations can differ, potentially involving different clinical subtypes of FTD, like BV-FTD, SV-PPA, NFV-PPA, PSP and CBD.[18]

The majority of known mutations in the coding region of MAPT predominantly occur within the microtubule-binding repeats.[27,28] These mutations lead to mutant tau proteins that exhibit reduced capability to bind microtubules.[27,28] Almost all coding-area mutations are found between exons 9 and 13.[23] In the case of intronic mutations, they tend to cluster around the 5′-splice site inside the intron following exon 10.[23] Both the intronic mutations and most of the exon 10 mutations affect the alternative splicing of exon 10's mRNA.[29,30] This leads to an increase in the production of 4R tau isoforms, which in turn, could result in an excess of tau that cannot bind to the limited available binding sites on microtubules, and eventually to the cytoplasmic deposition of unbound 4R tau.[23] Many mutations in the MAPT gene have been found in families with FTDP-17, some of which are: G27V, P301L, R406W [31] and N279K [32,33]. A representation of all MAPT mutations associated with FTDP-17 is shown in *Figure 2* as reviewed by Ghetti *et al.*, 2015.[23]

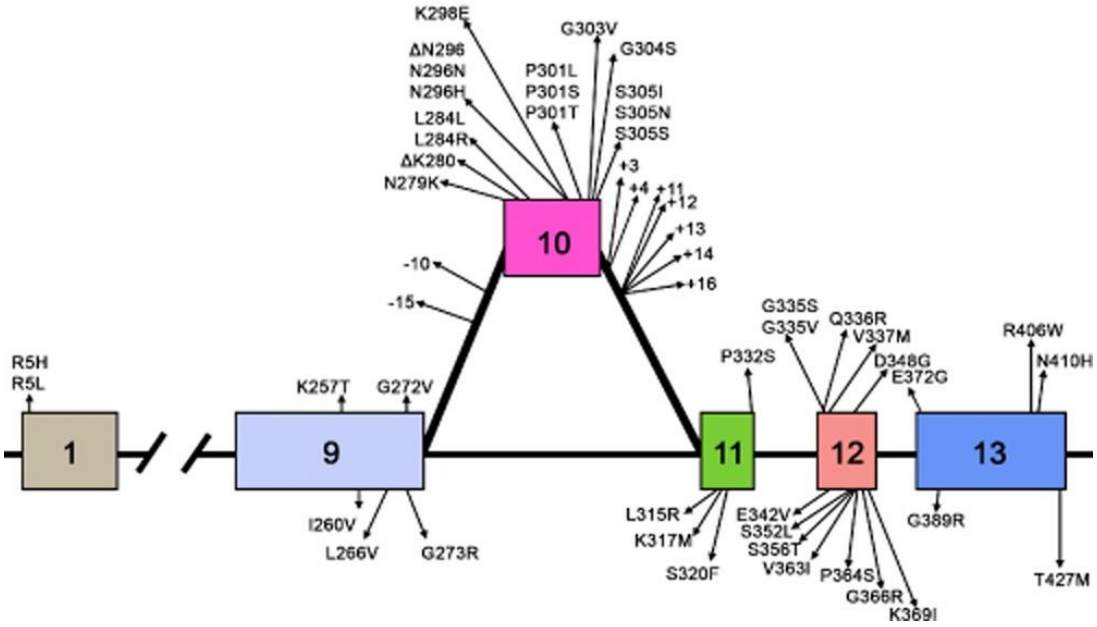

Figure 2: MAPT mutations associated with FTDP-17. 53 mutations causing FTDP-17 have been found inside the MAPT gene.[23]

Tau^{VLW} mouse model

The Tau^{VLW} transgenic mouse is a murine model of FTDP-17 that was used in the present study. Details around the methodology behind the production of these mice can be found in the Materials and Methods section, but briefly, these animals have a neuron-specific expression of the largest human Tau isoform that contains three mutations are linked with FTDP-17.[34] Tau^{VLW} mice express high levels of the mutant protein in the cortex and the hippocampus.[34] Their brains show higher concentration of hyperphosphorylated Tau protein, higher formation of Tau filaments and display lysosomal abnormalities.[34] Furthermore, these mice display a decrease of the ventral DG volume, a smaller number of DGCs of the ventral DG, a reduction in the number of proliferating cells in the ventral DG as well as an increase in cell death both in the dorsal and the ventral DG, compared to control mice.[35] Behaviourally, Tau^{VLW} mice present with depressive symptoms.[35] Additionally, this mouse model displays increased epileptic activity, prominent astrocytosis and activated microglia and augmented $GABA_A$ receptor-mediated hyperexcitability.[36] A more recent study showed that new-born DGCs of Tau^{VLW} mice have altered connectivity as they receive reduced excitatory and increased inhibitory innervation from local interneurons, changes that were partially reversed with environmental enrichment and chemo-activation.[37] New-born DGCs of TauVLW mice and of FTD patients showed similar alterations in their morphology, like reduced branching and reduced length of the primary apical dendrite.[37]

Treatment

Currently, there are no disease-modifying treatments approved by the FDA for FTD. The primary approaches to managing the disease involve environmental adjustments, caregiver education, mental and physical activities, speech therapy, and occupational and physical therapy.[38,39]

Selective serotonin reuptake inhibitors (SSRIs) have been shown to be beneficial for FTD patients. These medications have demonstrated improvements in functional measures and the management of behavioral symptoms such as disinhibition, apathy, stereotypies, agitation, and appetite changes.[40–44] Escitalopram and citalopram are generally preferred due to their better tolerability and lower risk of anticholinergic side effects.[41,45]

Dopamine-enhancing medications like methylphenidate, dextroamphetamine, and bromocriptine have shown promise in addressing risk-taking behavior, apathy, disinhibition, and speech problems in FTD patients.[46–48] Tetrabenazine has been effective in reducing severe tics and stereotypies in FTD.[49] Quetiapine being a preferred option for patients with parkinsonism due to its low D2 receptor blocking affinity.[50]

Several clinical trials are trying to target tau and TDP-43, offering potential therapeutic options for neurodegeneration. These trials involve anti-tau antibodies, tau phosphorylation and acetylation inhibitors, tau vaccines, and microtubule-stabilizing agents, each at various stages of development. One of them, that used a histone deacetylase inhibitor to elevate progranulin levels, reported no changes in the plasma or cerebrospinal fluid progranulin concentrations.[51] A different study that is using an inhibitor of tau aggregation is on phase III of its clinical trial, with no results being reported yet. (US National Institute of Health Clinical Trials Registry , 2013) A study in a transgenic tau mouse model used antibodies directed at altered conformations of tau and did report positive results with decrease in hyperphosphorylated, aggregated and insoluble tau levels.[52] Additionally, innovative gene-editing therapies using antisense oligonucleotides to reduce C9orf72 expansion in FTD are actively being investigated and developed.[53]

Hilar Mossy Cells

Dentate Gyrus

The mammalian hippocampal formation is divided into the Cornu ammonis (which is divided into the CA1, CA2 and CA3/CA4 areas), and the dentate gyrus (DG). The DG differs from the other hippocampal regions as it contains two (instead of one) principal glutamatergic cell types: the DGCs and the MCs. The DG has three layers: the molecular layer (ML), the granule cell layer (GCL), and the polymorphic layer or hilus. The ML does not contain many cells and is occupied mostly by the dendrites of the DGCs and the axons of the perforant pathway (PP), which project from the entorhinal cortex (EC). The GCL is comprised almost entirely of densely positioned DGCs. In the boundary of the GCL and the hilus, there is a region called subgranular zone (SGZ). Finally, the hilus which is enclosed by the GCL, contains MCs and distinct subtypes of interneurons. The anatomy of the DG is similar between rodents and primates.[54]

Trisynaptic Circuit

The trisynaptic circuit of the hippocampus involves three cell types: DGCs, pyramidal neurons of CA3, and pyramidal neurons of CA1. The initial connection happens between the EC and the DG. The EC sends signals from the parahippocampal gyrus to the DG through DGC fibers collectively known as the PP. From there, the DG connects to pyramidal cells of CA3 through MC fibers. CA3, in turn, transmits signals to CA1 via Schaffer collaterals, which synapse in the subiculum and are then carried out through the fornix.[55] Together, the DG, CA1, and CA3 in the hippocampus make up the trisynaptic loop (*Figure 3*). Even though the trisynaptic circuit is a simplification of hippocampal functional connectivity, it includes the most important characteristics of the structure.

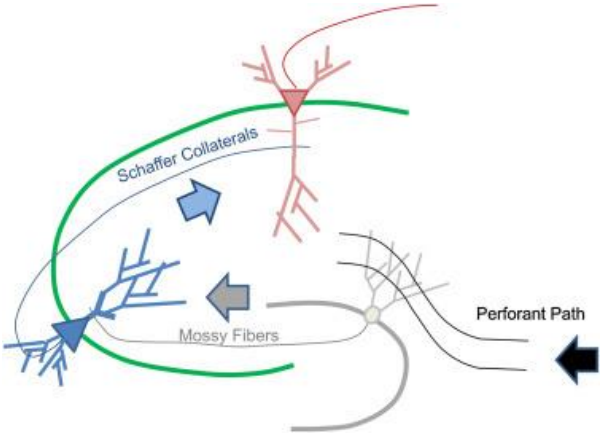

Figure 3: The trisynaptic circuit. The EC projects to the DG via the PP (1st synapse), the DG projects to CA3 via mossy fibres (2nd synapse) and the CA3 projects to CA1 via Schaffer collaterals (3rd synapse).[56]

Mossy Cell characteristics

MCs are a common hilar cell type, as they make up more than 30% of hilar cells in rodents.[57,58] The bodies of MCs are relatively large (~30µm in rodents) and have a triangular or multipolar shape.[54] Multiple apical dendrites emerge from the cell bodies and extend distally within the hilus.[59,60] Typically, each main dendrite splits once or twice, giving rise to more, smaller branches, and thus creating an extended dendritic tree.[54,60] Most of these branches stay inside the hilus, however some dendrites enter the ML.[54,61] The most distinctive characteristic of MCs is that their proximal dendrites have large and intricate spines which are called thorny excrescences and give the cells their typical "mossy" appearance. These excrescences are the termination points for the mossy fiber axons (the axons of DGCs), with the synapse being established between the large boutons of DGCs containing glutamatergic vesicles and the MCs thorny excrescences.[60,61] The more distal dendrites of MCs show more typical spines, that are not densely distributed.[54]

Concerning the axon of the MC, they project distally to both the ipsilateral and contralateral DG.[62,63] These distal projections terminate mostly in the inner ML, with the terminals mostly innervating DGC dendritic spines, since dendrite-containing interneurons in the inner ML rarely have spines.[62] The axons of MCs can also collateralize and project to other areas of the ML (medial and outer).[59,62] MCs also have

axon collaterals near the cell body, which innervate the inner ML.[64] As it is described in this paragraph, MCs project to distinct areas of the DG, which is probably one of the reasons why their actual function is not yet entirely understood.

Mossy Cell function

Early studies have shown that MCs are glutamatergic.[65,66] They both activate[66,67] and indirectly inhibit[67,68] DGCs by activating GABAergic interneurons. They both receive afferents and project back to GCs locally/ipsilaterally, contralaterally, and across the whole longitudinal axis of the hippocampus. As a result, they create a positive-feedback loop. Their synapses with GABAergic interneurons facilitate a feed-forward inhibition on DGCs. However, whether overall inhibition or excitation prevails, is not yet answered. The main problem scientists face while trying to answer this question, is that MCs are hard to selectively activate with electrophysiology methods, since their axons and dendrites are located very close to other DGCs and axonal projections. One of the first studies that attempted to study this effect recorded pairs of monosynaptically connected MCs and DGCs.[67] This paper showed that MCs excited DGCs, but excitatory postsynaptic potential (EPSP) could be detected only when GABAergic interneurons were blocked with a GABA-A receptor antagonist. Since there were frequent failures of synaptic transmission, the excitatory function of MCs on DGCs seemed to be weak, thus suggesting that the overall effect of MCs is the inhibition of DGCs. However, when the DGC was already depolarized, the excitatory effect of the presynaptic MC was larger, concluding that MCs can have an excitatory effect on already depolarized DGCs.[67] A different group lesioned specifically MCs in hippocampal slices and found a decrease in the excitability of DGCs when the PP was stimulated, thus supporting that MC effect on DGCs is overall excitatory.[69] Many studies over the last decades have tried to answer this question but the overall role of MCs is still debated both in normal and pathological conditions.

MCs are distinct from the other cell types of the DG, as they produce frequent spontaneous EPSPs, which can initiate action potentials.[70–72] Furthermore, MCs express the immediate early gene c-fos even without behavioural stimulation, whereas most other hippocampal neurons need this stimulation to express c-fos.[73]

MCs are involved in hippocampal synaptic plasticity. The input from DGCs to MCs shows long term potentiation (LTP).[74–77] A study has found NMDA receptor-independent LTP as well as activity-dependent short-term modification functions (frequency-dependent facilitation, burst facilitation) on mossy fiber synapses.[74] Other groups have demonstrated that the MC to DGC synapse also displays a form of LTP, which is NMDA receptor-independent and involves presynaptic cAMP/PKA signalling and postsynaptic BDNF/TrkB signaling.[75–77]

Another aspect of MCs function is their involvement in pattern separation. Pattern separation refers to the process through which inputs or representations that overlap or closely resemble each other are converted into outputs that are less similar, and it is a function very important for episodic memory.[78,79]

The role of DGCs in pattern separation is extensively studied. They receive different sensory inputs from the EC through the PP, and with the synapses between the DGCs being infrequent, they allow for the temporal separation of information transmission. [80,81] In addition, DGCs display a poor firing pattern and showed either no, or only one, space field in a specific environment.[82] The role of MCs in pattern separation, on the other hand, has not been thoroughly studied, even though they constitute a major cell type of the DG. Some recent studies showed that MCs, in contrast to DGCs, have a very active firing pattern, many place fields and displayed remapping during exploration of different environments.[82,83] The authors propose that MCs and DGCs work in a synergistic way for DG pattern separation. They suggest that MCs control the excitability, scarcity, and activity of DGCs. By activating nearby interneurons, MCs may control that only the most active DGCs have firing fields, thus maintaining a level of sparsity in GC activity that is necessary to facilitate pattern separation.[82]

Furthermore, MCs are involved in the regulation of adult hippocampal neurogenesis (AHN). AHN is the process through which new neurons are born and incorporated into the hippocampal network throughout life. This process takes place in several mammalian species, including humans.[84–86] Maturation of new-born DGCs, as well as their synaptic integration in the existing network of the DG is regulated by the first synapses that those cells receive. It has been suggested that MCs play a significant role in these processes by providing immature DGCs their initial glutamatergic synapses.[87] Additionally, it has been shown that MCs can influence the quiescence or activation of neural stem cells (NSC) by directly exciting or indirectly inhibiting these cells.[88] In the same study, when MCs were genetically removed, the NSC population was reduced and AHN was negatively affected.[88] Additionally, MCs release the signalling protein Sonic hedgehog (Shh), which is important for the proliferation of neural precursors and the migration of immature neurons in the SGZ.[89] A more recent study (pre-print, not yet peer-reviewed) showed that the deletion of Shh from MCs advanced the age-related decrease of the NSC population and impaired NSC self-renewal.[90]

Roles of MCs under pathological conditions

Temporal Lobe Epilepsy

Temporal Lobe Epilepsy (TLE) is the pathological condition most associated with hilar MCs. Consequently, this is the pathological context in which these cells have been studied. This disorder involves seizures that start in the temporal lobe and is characterized by extensive loss of neurons in the hippocampus, which has been described both in human patients and animal models of the disease.[91,92] MCs, together with somatostatin-positive hilar PP-associated interneurons (HIPP cells), are the most affected type of neurons in TLE.[53] The assumption behind MC vulnerability in TLE arises from their sensitivity to excitotoxicity. DGC buttons that project on MCs release large amounts of glutamate during seizures, which leads MCs to be continuously depolarised.[93] Furthermore, MCs could be sensitive to excitotoxicity since they lack sufficient intracellular calcium trafficking due to low expression levels of

calcium-binding proteins.[94] Other studies suggest that MCs show a low level of autophagy, which could be harmful in conditions of intense metabolic processes.[95]

The mechanism through which the loss of MCs leads, or contributes to, TLE is still under investigation. It is hypothesized that hilar basket cells lose their excitatory input from MCs, and as a result, DGCs are disinhibited.[96] However, this suggestion is debated since HIPP cell number is decreased during TLE, as mentioned before, and the loss of these GABAergic interneurons might also contribute to DGC disinhibition-hyperexcitability.[97,98] Another hypothesis postulates that the surviving MCs in TLE become hyperactive and cause DGC hyperexcitability. These remaining MCs show increased excitability and spontaneous burst discharges.[99–101]

Schizophrenia

MCs have been suggested to be involved in the development of schizophrenia (SCZ). SCZ is a psychiatric condition marked by persistent or recurring episodes of psychosis, with the most common symptoms being hallucinations, delusions, disordered thought patterns and social behaviour problems.[102] DTNBP1 (dystrobrevin-binding protein 1), which encodes dysbindin-1, is an important risk gene for SCZ.[103,104] This protein, and specifically its 1C isoform, is expressed by MCs. The expression levels of this isoform and those of the isoform 1B are decreased in schizophrenic hippocampi, while the levels of isoform 1A do not show any changes.[105] A study that used a mouse model of SCZ (sdy mice, in which dysbindin-1A and -1C are deleted) showed that a possible mechanism leading to SCZ could be altered AHN.[106] They demonstrated that these mice have a delayed maturation of new-born neurons, which was suggested to be caused by the loss of MCs that followed the dysbindin-1C deficiency.[106] The same team, a year later, suggested that the mechanism behind the loss of MCs in sdy mice is the impaired autophagy caused by dysbindin-1C deficiency.[95] They showed no changes in the signals of apoptosis in the SCZ mouse model but found decreased levels of LC3-II (marker of autophagosomes) in the hippocampi of these mice.[95]

Alzheimer's Disease

In the last few years, MCs have been studied in the context of AD as well. AD is a tauopathy, as mentioned before, and apart from the accumulation of tau protein, it is also marked by the progressive accumulation of amyloid beta (Aβ). It has been suggested that, in early stages of the disease, Aβ accumulation may be caused by hippocampal network hyperexcitability.[107] A recent study used an AD transgenic mouse model (Tg2576) at an early age, to show that MCs of these mice have increased excitability (increased EPSP frequency, more action potentials, depolarized resting membrane potential) and strong intracellular Aβ accumulation.[108] Another study using a different AD mouse model (3xTg-AD) demonstrated that MCs show increased levels of hyperphosphorylated (pT205 and pT231) and truncated tau (hTau N368).[109] When hTau was specifically overexpressed in ventral MCs, mice showed spatial cognitive deficits, which were caused by disruption of the dorso-ventral communication.[109] Later,

the chemo-genetic activation of MCs improved the impairments in spatial cognition.[109] RNA-seq revealed that several AD-related signaling pathways were disrupted in the hTau N368 overexpressing cells, like decrease in synapse-associated proteins (PSD95, GluA1, GluA2, GluN2A, GluN2B) and decrease in phosphorylated protein kinase B (pPKB) and phosphorylated glycogen synthase kinase-3β (pGSK-3β).[109] Another study showed that, in an AD mouse model, (APPswe/PSEN1dE9), the synapse between MC and HIPP cell is dysfunctional and causes memory imprecision.[110] They found that miR-128 (inhibitor of STIM2 translation) has increased expression levels in MCs of these mice, and that silencing this miRNA, and therefore restoring STIM2 expression, leads to rescuing synaptic function and memory imprecision.[110] Taken together, these results show that MCs are altered in the early stages of AD. However, the exact molecular mechanisms behind MC dysfunction in AD and other tauopathies are yet to be discovered.

Molecular Markers

One of the main difficulties pertaining MC research is the lack of cell specific markers. In *Table 1*, the main molecular markers that label MCs are summarized. In this table, information about each marker are displayed, as well as the species in which expression in MCs has been reported. The markers chosen for the present project are CR, Dysbindin-1C, CART and D2R, since, according to the current literature, they are the most selective markers for MC.

Table 1: Molecular markers of hilar Mossy Cells.

Molecular Marker	Marker Details	Species where MCs are labeled
CR	Calretinin. Calcium-binding protein, intracellular calcium signaling,	Mouse (ventral DG)[111–113], Nonhuman primates[114]
Dysbindin-1C	Dystrobrevin-binding protein 1, isoform C. Promotion of cell growth and proliferation, protection against apoptosis, regulation of intracellular protein transport.	Mouse[106]
D2R	Dopamine receptor D2. Coupled to Gi protein, receptor for most antipsychotic drugs.	Mouse[115]
CART	Cocaine- and amphetamine-regulated transcript. Involved in reward, appetite regulation and stress response.	Human[116]
GluR2/GluR3	Glutamate receptor AMPA type subunit 2/3. Most common excitatory neurotransmitter receptor in the CNS.	Rat[117], Nonhuman primates[65]
CGRP	Calcitonin gene-related peptide. Regulation of appetite, transmission of nociception.	Rat[118]
CB1R	Cannabinoid receptor type 1. (Mostly) coupled to Gi/o proteins. Activation by endocannabinoids or exogenous cannabinoids.	Mouse, Rat[119]
p11	S100 calcium-binding protein A10. Transport of neurotransmitters, mood regulation.	Mouse[120]
SMARCA3	Helicase-like transcription factor. Chromatin-remodeling factor, regulation of transcription.	Mouse[120]

GR type 2	Glucocorticoid receptor type 2. Receptor to receptor of cortisol and other glucocorticoids. Regulation of gene transcription.	Mouse, Rat[121]
STEP	Striatal-enriched protein tyrosine phosphatase. Regulation of the extracellular signal-regulated kinase pathway.	Mouse[122]

CR is the most typical MC marker in mice. Several studies have reported its immunoreactivity in the mouse DG.[111–113] Most studies that have been published so far report that CR is only expressed by the MCs of the ventral DG and that its expression in the dorsal part is limited.[111,113] Apart from MCs, CR is also expressed by immature DGCs, which are located in the SGZ, and by a population of hilar interneurons.[111,113] In the human DG, very few studies have used CR, and these have reported that human MCs do not express CR.[114,123] In these studies, CR-expressing hilar neurons are categorized as interneurons.[116,123] However, those papers support that MCs are CR immunoreactive in other primates, similarly to mouse MCs.[114] A different study suggested that the differences observed between human and non-human primates are due to methodological differences and not true interspecies variations.[124] As mentioned previously, dysbindin-1C is another common marker for MCs in the mouse DG. Several groups have used it to label MCs, and it has been shown to be essential for MC survival.[105,106] One study has also reported that human MCs express dysbindin-1C.[125] CART is a neuropeptide that is expressed by MCs of the human DG.[116] Mouse MCs have not been reported to express this specific marker. Finally, D2R is expressed by mouse MCs according to published literature.[115] In fact, a recent study showed that when the D2R gene was removed from MCs, there was impairment is spatial memory and increased anxiety.[126]

Materials and Methods

Animals

The Tau^{VLW} transgenic mouse model was established by Dr Jesus Ávila's laboratory to investigate the mechanisms underlying neurodegeneration resulting from Tau alterations.[34] These mice harbour three distinct mutations (G272V, P301L, and R406W) in the human MAPT gene, which have been associated with familial forms of FTD-Tau. These mutations were introduced through site-directed mutagenesis, utilizing the pSGT42 plasmid containing a human four-repeat Tau cDNA isoform with two N-terminal exons. Neuronal-specific expression of human Tau cDNA was achieved by integrating it into a murine Thy1 expression cassette (*Figure 4*).

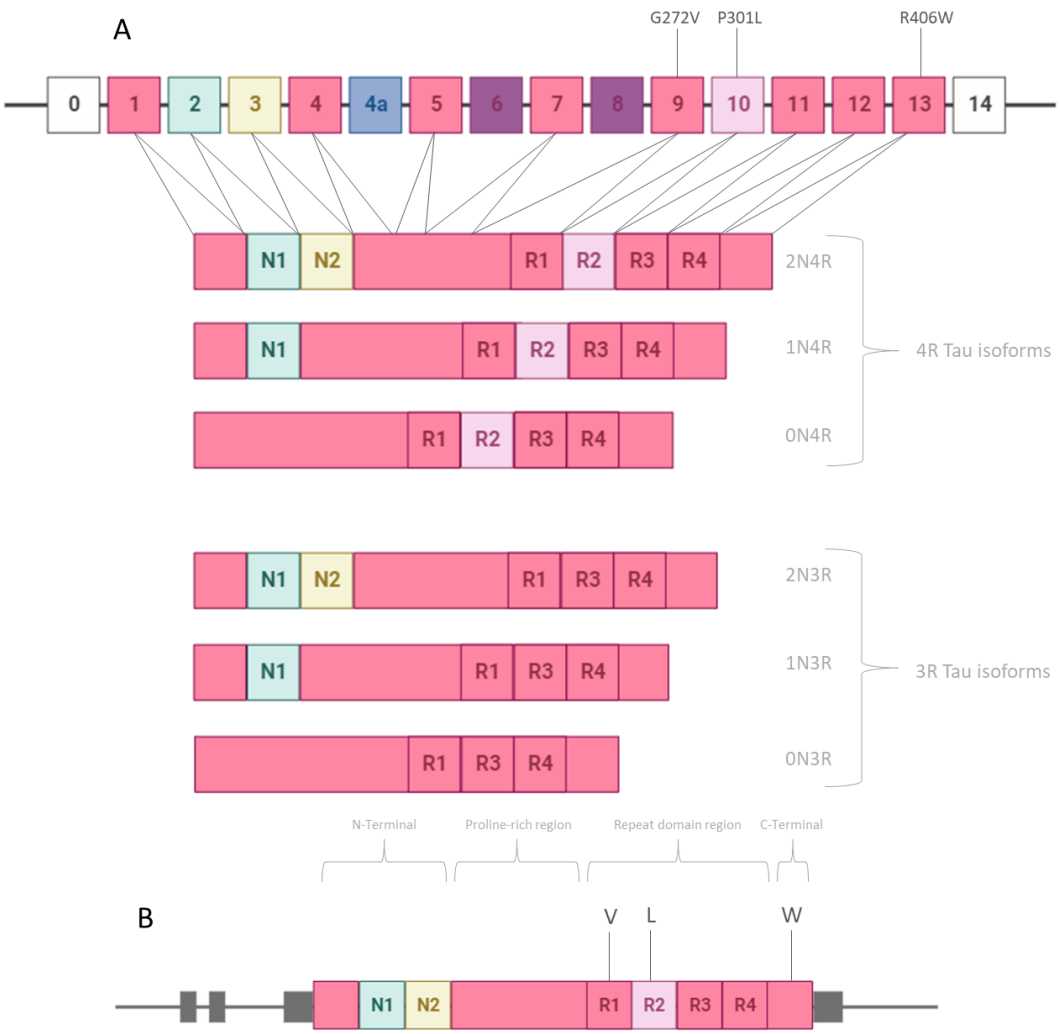

Figure 4: MAPT gene and VLW transgene. A: MAPT gene and human Tau isoforms. Top: MAPT gene exons with three mutations associated with FTDP-17. Bottom: 6 Tau isoforms in the human CNS. B: VLW transgene containing 3 mutations, created with site-directed mutagenesis. Neuron-specific expression is guided with the Thy1 gene promoter cassette (grey). Figure created with Biorender.

For this study, we utilized a cohort of 7 female 4-month-old Tau^{VLW} mice alongside 7 age-matched female C57/BL6J control mice. Both Tau^{VLW} and wild-type littermates were bred and maintained within a specific pathogen-free colony facility at the Centro de Biología Molecular "Severo Ochoa" (CBMSO). The animals were housed under controlled conditions with a temperature of 22 ± 1 °C, a 12/12 hours light/dark cycle, and *ad libitum* access to food and water. Housing conditions and experimental procedures adhered rigorously to the European Community Guidelines (directive 86/609/EEC) for laboratory animal care. All animal handling strictly followed the guidelines set forth by the national animal welfare bodies of Autonomous University of Madrid and CSIC and of the Higher Scientific Research Council. All animal research received approval from the Bioethics Committee of the Centre for Molecular Biology Severo Ochoa. Animal experiments were approved by the CBMSO (AEEC-CBMSO-23/172) and the National (PROEX 205/15 and PROEX 185.4/20) Ethics Committees.

Sacrifice of animals

16-week-old mice were deeply anesthetized through intraperitoneal injection of pentobarbital (EutaLender, 60 mg/kg). The absence of foot and tail reflexes was meticulously confirmed before proceeding with perfusion. Transcardial perfusion was conducted using 50 mL of 0.9% saline buffer (0.9g NaCl/100mL H_2O) followed by 50 mL of 4% paraformaldehyde in 0.1N phosphate buffer (PB). The excised brains were post-fixed at 4°C overnight (16-20 hours) in 4% paraformaldehyde in 0.1N PB, followed by triple rinsing in 0.1N PB on the subsequent day.

Tissue processing

Animal brains were cut along the interhemispheric fissure, separating the two hemispheres. Each of the hemispheres was immersed in a 10% sucrose–4% agarose solution to increase tissue robustness and prevent tissue damage and to ensure cutting of the whole tissue. 50 µm thick, sagittal sections were obtained from both hemispheres on a Leica VT1200S vibratome. Series of sections were generated with every 9th section. The series of sections were initially placed in 0.1 N PB, briefly dried on absorbent paper and then kept in a cryo-preservative solution (30% polyethylene glycol, 10% 0.2 N PB, 30% glycerol, and 30% bi-distilled water) housed in 24 well-plates at -20°C for future use. All series of sections that were used for this project were sourced from the left hemisphere.

Nissl staining

One series of slices obtained from the left hemisphere (picked randomly) of each mouse was used for Nissl staining. For each series of sections sampling probability was 1/8. Only for this part of the project, we used 10 additional series of slices (obtained from 5 Tau^{VLW} mice and 5 C57/BL6J control mice). These series were obtained in the past by different members of the lab and stored at -20°C, in a cryo-preservative solution. As a result, Nissl staining was performed for 24 series of slices (7+5 Tau^{VLW} mice, 7+5 control mice) using the following protocol:

Each series of slices was mounted on gelatine-coated glass slides, and air dried for 48 hours. The desiccated microscope slides were then subjected to a series of sequential treatments. Initially, the slides were immersed in an aqueous solution of Toluidine Blue, a basic thiazine dye, for 8 minutes. Following this step, the slides were submerged in distilled water for a brief interval of 10 seconds to remove excess dye residues. Subsequently, the slides were subjected to a gradual dehydration process involving ethanol of varying concentrations. Specifically, the slides were immersed in 70% ethanol solution for 2 minutes, facilitating the initial stabilization of cellular structures. This was followed by immersion in a 96% ethanol solution for another 2-minute interval, which contributed to further dehydration and preservation of the sample. A subsequent treatment involving 100% ethanol was performed twice, each instance spanning 2 minutes, to ensure optimal dehydration and removal of residual water. Consequent to the ethanol treatments, a solution of xylene was used in a 2-minute immersion step, serving as a clearing agent to render the samples transparent. After the clearing process, a small quantity of DEPEX, a synthetic mounting medium, was applied onto a 60*40mm coverslip. The coverslip was subsequently

delicately placed on the prepared slide. The assembled slides were allowed to undergo a drying period of 3 days within a fume cabinet, providing a controlled environment conducive to the evaporation of solvents and the establishment of a stable mounted specimen.

Acquisition of images

Scans of the entire glass slide, containing a series of slices for each mouse, were obtained using a Leica DMI8 microscope, connected to a Leica-DFC9000GT-VSC14757 camera. For image acquisition the LAS X software was used. A 5X objective was used and the XY dimensions for each scanned area were 2,661.1 μm*2,661.1 μm. After determining different focus points (z positions concentrating on the DG) for each slice, tile scans of all slices were obtained. For every animal, 9-12 scans were obtained, in 6-8 of which, the formation of the DG was present.

Dentate Gyrus and Hilus Volume Estimation

As mentioned before, both hemispheres of mouse brains were cut from the lateral-most to the medial-most part, so each series included slices encompassing the entire hippocampus of each mouse. Those slices range from the position where the dentate gyrus is not yet present (3.925 mm lateral) to the midline (0.00 mm lateral). To examine the dorsal and ventral dentate gyrus separately, three distinct regions were taken into account. The most lateral area consisted of sagittal slices that ranged between 3.325 mm and 2.725 mm, where the dentate gyrus appears as an individual structure. In this area, the DG was equally split in a dorsal and a ventral part, both of which were analysed separately. The subsequent region (located closer to the midline) included slices from 2.725 mm to 1.95 mm lateral positions. In this area, the dorsal and ventral parts of the DG appear as distinct structures and are clearly discernible. The third and most medial section of the hemisphere was composed of slices ranging from 1.95 mm lateral to the midline. As the ventral segment of the DG is absent in these slices, only the dorsal section was analysed. The hilus in both the dorsal and the ventral part, was distinguished as the area extending from the SGZ until the CA3 field. The volumes of the dorsal and ventral DG and hilus were evaluated stereologically, using the freehand selection tool of the Fiji software and by employing the Cavalieri method[127] on each series of Nissl-stained sections. In that end, all the areas that were measured for each mouse were summed and the resulting surface was multiplied by 400μm (50μm thick slices*8, as each series were generated with every 9th section): $Volume\ (\mu m^3) = Sum\ of\ all\ areas\ (\mu m^2) * 400 \mu m.$ This formula was used to calculate the volumes of both dorsal and ventral parts of the DG.

Human subjects

In total, 18 human subjects were encompassed in this study, comprising 13 control individuals and 5 subjects with FTD. The use of brain tissue samples was organised by the local brain bank (Banco de Tejidos CIEN, Madrid, Spain), following national laws and international ethical and technical guidelines on the use of human samples for biomedical research purposes. Samples were collected at the Banco de Tejidos CIEN (Madrid, Spain), the Hospital Clínico Universitario Virgen de la Arrixaca (Murcia, Spain), the Biobanco del Hospital Universitario Reina Sofia (Córdoba, Spain), and the Instituto

Anatómico Forense (Madrid, Spain). The entire process, encompassing brain tissue donation, processing, and research utilization, was conducted in alignment with established guidelines. Informed consent was obtained from living donors, and the Ethical Committee of the Banco de Tejidos CIEN granted approval (committee approval reference 15-20130110). Tau phosphorylation in the anterior hippocampus, in the parietal, prefrontal, temporal associative isocortex and in the primary visual cortex was measured at the neuropathology department of the Banco de Tejidos CIEN to determine each subject's Braak stage. All the neurologically healthy individuals included in this project were at Braak stage 0. *Table* 2 includes the epidemiological data of the all subjects.

Table 2: Clinical, epidemiological, histological and fixation data of 15 neurologically healthy subjects and 5 FTD patients.

Subject	Clinical Diagnosis	Age	Gender	PMD (Hours)	Cause of Death	Fixative	Braak Tau Stage	TDP-43
CONTROL 1	CONTROL	52	FEMALE	6	Cancer	4% PFA, 24 h at 4 ºC	0	NEGATIVE
CONTROL 2	CONTROL	43	MALE	5	Leukemia	4% PFA, 24 h at 4 ºC	0	NEGATIVE
CONTROL 3	CONTROL	68	MALE	4	Respiratory infection	4% PFA, 24 h at 4 ºC	0	NEGATIVE
CONTROL 4	CONTROL	83	FEMALE	4	Stroke	4% PFA, 24 h at 4 ºC	0	NEGATIVE
CONTROL 5	CONTROL	61	MALE	8	Digestive hemorragia	4% PFA, 24 h at 4 ºC	0	NEGATIVE
CONTROL 6	CONTROL	61	FEMALE	8	Cancer	4% PFA, 24 h at 4 ºC	0	NEGATIVE
CONTROL 7	CONTROL	65	MALE	18	Stroke	4% PFA, 24 h at 4 ºC	0	NEGATIVE
CONTROL 8	CONTROL	63	MALE	38	Stroke	4% PFA, 24 h at 4 ºC	0	NEGATIVE
CONTROL 9	CONTROL	87	MALE	6.5	Sepsis	4% PFA, 24 h at 4 ºC	0	NEGATIVE
CONTROL 10	CONTROL	86	MALE	7	Ventilatory failure	4% PFA, 24 h at 4 ºC	I	NEGATIVE
CONTROL 11	CONTROL	74	FEMALE	8	Cancer (Carcinoma pancreas)	4% PFA, 24 h at 4 ºC	I	NEGATIVE
CONTROL 14	CONTROL	75	FEMALE	5	Cancer	4% PFA, 24 h at 4 ºC	0	NEGATIVE
CONTROL 15	CONTROL	78	MALE	3	Aortic dissection	4% PFA, 24 h at 4 ºC	0	NEGATIVE
FTD 1	FRONTOTEMPORAL DEMENTIA	76	MALE	5	Unknown	4% PFA, 24 h at 4 ºC	II	NEGATIVE
FTD 2	FRONTOTEMPORAL DEMENTIA	71	MALE	4	Respiratory infection	4% PFA, 24 h at 4 ºC	0	POSITIVE
FTD 3	FRONTOTEMPORAL DEMENTIA	73	MALE	9	Cardiorespiratory failure	4% PFA, 24 h at 4 ºC	I	POSITIVE
FTD 4	FRONTOTEMPORAL DEMENTIA	56	FEMALE	<12	Cardiorespiratory failure	4% PFA, 24 h at 4 ºC	NA	POSITIVE
FTD 5	FRONTOTEMPORAL DEMENTIA	64	MALE	7	Multi-organic Failure	4% PFA, 24 h at 4 ºC	VI	NEGATIVE

Tissue processing

After extracting the brain, the hemispheres were separated with a mid-sagittal section. All hippocampal samples for this study came from the right hemisphere. Following a previously established procedure, a 0.5-1 cm-thick block of hippocampal tissue, corresponding to the posterior part of the anterior hippocampus, was swiftly dissected on ice and immediately placed in freshly prepared 4% paraformaldehyde (PFA). External anatomical landmarks were used to select the sampling region to avoid potential biases from hippocampal atrophy and ensure uniformity across all subjects. Furthermore, all autopsies were conducted by the same pathologist. The PFA fixative solution, with a pH of 7.4, was freshly prepared just before the autopsy by diluting a commercial 16% PFA solution (Electron Microscopy Sciences) in 0.2 N phosphate buffer (PB) and distilled water in a 1:2:1 ratio. All samples were fixed for a maximum of 24 hours at 4ºC and rinsed three times in 0.1 N PB before immediate sectioning.

Hippocampal tissue blocks were immersed in a solution of 10% sucrose and 4% agarose in a 12-well plastic plate. The plate was then chilled on ice until the sucrose-agarose had solidified completely. Subsequently, a cubic block of the hippocampus embedded in sucrose-agarose was shaped and cut using a Leica VT-1200S sliding blade vibratome, resulting in 50 µm-thick sections. These hippocampal

sections were promptly stored at -20ºC in 24-well plastic plates containing a cryo-preservative solution (30% polyethylene glycol, 10% 0.2 N PB, 30% glycerol, and 30% distilled water).

Immunohistochemistry

Mouse samples

For specific marker detection in the mouse DG, series of brain slices were made up of one section from every ninth, as mentioned before. One series of slices obtained from the left hemisphere of each mouse (7 Tau^{VLW}, 7 C57/BL6J mice) was used for immunohistochemistry. Each series was initially incubated in PB 0.1N and rinsed three times before proceeding with the experimental protocol.

After a series of antibody tests to determine the optimal experimental conditions, it was decided to perform a heat-mediated citrate buffer antigen retrieval (AR) step, to improve the antibody signal (especially for the Dysbindin marker). The AR step was performed in 10 mL glass vials. The series of sections of each mouse was incubated in 5 mL of preheated 1× citrate buffer (pH 6.0) antigen retrieval solution (Vector, H-3300). The 10× antigen retrieval stock solution was diluted in distilled H_2O. Then, vials were exposed to 5–6 brief (5-10 seconds) cycles of microwave heating. Boiling of the liquid was avoided to prevent tissue damage. Next, vials were tightly closed and immersed in an 80 °C water bath for 20 min. Finally, closed vials were left at room temperature for an additional 20 min and washed 5 times in PB 0.1N, before proceeding to the immunohistochemistry procedure.

After the antigen retrieval step, double immunohistochemistry was performed using the following primary antibodies: rabbit anti-Dysbindin (Polyclonal, 1:500 dilution, Proteintech, Cat No. 11132-1-AP) and guinea pig anti-Calretinin (Polyclonal, 1:500 dilution, Synaptic Systems, Cat No. 214104). The samples were incubated with the primary antibodies under gentle shaking at 4°C for 48 hours. To detect the binding of primary antibodies, Alexa Fluor-488 donkey anti-rabbit (1:1000 dilution Thermo Fisher Scientific, Cat No. A-21206) and Alexa Fluor-555 goat anti-guinea pig (1:1000 dilution, Thermo Fisher Scientific, Cat No. A-21435) secondary antibodies were used. The samples were incubated with the secondary antibodies under gentle shaking at 4 °C for 24 hours. Primary and secondary antibodies were diluted in a blocking buffer (PB 0.1N with 1% Triton X-100, 1% BSA). All sections were counterstained for 10 minutes with 4’,6-diamidino-2-phenylindole (DAPI, Merck, 1:5000 dilution) to label cell nuclei. Finally, each series of slices was mounted on gelatine-coated glass slides. A non-commercial anti-fading mounting medium (33% glycerol and 7.5% Mowiol, prepared in 0.2 M Tris-HCl, pH 8.5) was used to embed the sections. Slides were left to dry for 24 hours and stored in opaque microscope slide cages, as to be protected from light.

Human samples

Immunohistochemistry and acquisition of confocal images for the human subjects that were used to count the number of CR positive cells were performed in cooperation with Moreno Jiménez Elena. Briefly, slices were initially incubated in PB 0.1N and rinsed three times. To remove the

autofluorescence caused by aldehyde fixation, samples were incubated in a 0.5% sodium borohydride ($NaBH_4$) solution (diluted in 0.1 N PB) under gentle shaking for 30 min, and were rinsed 5 times in 0.1 N PB afterwards. A mild heat-mediated citrate buffer AR step was performed following the same protocol that was used for mouse slices. Samples were rinsed 5 times in 0.1 N PB after the AR step. Double IHC was performed with the following primary antibodies: rabbit anti-CR (Polyclonal, Swant, Cat No. CR 7697) and mouse anti-Polysialylated-neural cell adhesion molecule (PSA-NCAM) (Monoclonal, 1:1000 dilution, Millipore, Cat No. MAB5324). The samples were incubated with the primary antibodies under gentle shaking at 4°C for 5 days. To detect the binding of primary antibodies, Alexa Fluor-488 donkey anti-rabbit (1:1000 dilution, Thermo Fisher Scientific, Cat No. A-21206) and Alexa Fluor-647 donkey anti-mouse (1:1000 dilution, Thermo Fisher Scientific, Cat No. A-31571) secondary antibodies were used. The samples were incubated with the secondary antibodies under gentle shaking at 4 °C, for 24 hours. The dilution of both the primary and the secondary antibodies was done in a blocking buffer (PB 0.1N with 1% Triton X-100, 1% BSA). After incubation with secondary antibodies, sections were rinsed 3 times in 0.1 N PB and counterstained for 10 min with DAPI (Merck, 1:5000 dilution) to label cell nuclei. IHC was followed by a final autofluorescence elimination step. To this end, a commercial Autofluorescence Eliminator reagent (EMD Millipore) was used, following the manufacturer's instructions. Sections were mounted on gelatine-coated glass slides. A non-commercial anti-fading mounting medium (33% glycerol and 7.5% mowiol, prepared in Tris-HCl 0.2 M pH = 8.5) was used to embed the sections. Slides were left to dry for 24-48 hours and protected from light in opaque microscope slide cages. Confocal images were acquired within one month after mounting to prevent any reduction in the intensity of the fluorescent signal and to ensure homogeneity in the time elapsed for all the subjects.

To further assess the phenotype of CR-immunoreactive cells that we observed in the human DG, we performed additional immunohistochemistry experiments using other well-validated markers of hilar MCs. The primary antibodies that were used for this part of the project were: rabbit anti-Dysbindin (Polyclonal, 1:500 dilution, Proteintech, Cat No. 11132-1-AP), guinea pig anti-CR (Polyclonal, 1:500 dilution, Synaptic Systems, Cat No. 214104), rabbit anti-D2R (Polyclonal, 1:500 dilution, Abcam, Cat No. ab150532), goat anti-CART (Polyclonal, 1:500 dilution, R&D systems, Cat No. AF163), rabbit anti-DCX (1:500 dilution, Abcam, Cat No. 207175) and mouse anti-DCX (Monoclonal, 1:50 dilution, Santa Cruz, Cat No. sc271390). To detect the binding of primary antibodies, Alexa Fluor-555 donkey anti-goat (1:1000 dilution, Thermo Fisher Scientific, Cat No. A-21432), Alexa Fluor-647 donkey anti-rabbit (1:1000 dilution, Thermo Fisher Scientific, Cat No. A-31573), Alexa Fluor-555 donkey anti-rabbit (1:1000 dilution, Thermo Fisher Scientific, Cat No. A-31572), Alexa Fluor-488 donkey anti-guinea pig (1:1000 dilution, Jackson ImmunoResearch, Cat No. 706-545-148) and Alexa Fluor-647 donkey anti-mouse (1:1000 dilution, Thermo Fisher Scientific, Cat No. A-31571) secondary antibodies were used. The dilution of both the primary and the secondary antibodies was done in a blocking buffer (PB 0.1N

with 1% Triton X-100, 1% BSA). We used the same immunohistochemistry protocol that is described in the previous paragraph (including the $NaBH_4$, the AR and the autofluorescence elimination steps).

Acquisition of confocal images

Images obtained from mouse samples

Confocal stacks of images were obtained in a LSM900 Zeiss confocal microscope. 5-7 stacks in the dorsal area and 5 stacks in the ventral area of the DG, per animal, were used to stereologically estimate the density of CR^+ and $Dysbindin^+$ cells. All stacks were obtained under a 63X objective, with 1.5 zoom, XY dimensions: 67.61 µm, thickness of z-stack at 25µm and z interval of 0.4µm. For the dorsal area, 1 stack was obtained from each section per mouse. For the ventral region, since it is not present in all the sections, images were randomly obtained from a minimum of 3 sections per animal. The DG, and subsequently the hilus, were first identified using a 10X dry objective in the DAPI channel. Next, stacks of images of the hilus were obtained at randomly selected locations. Only the DAPI channel was visualized when selecting these locations. IHC, image acquisition, cell counts and image analyses were performed blind to the genotype of the animals.

Images of human samples

Confocal stacks of images were obtained in an Olympus Spinning Disk Confocal SpinSR10 coupled to an inverted IX83 microscope. 5 stacks per subject were used to stereologically estimate the density of CR^+ cells. All stacks were obtained under a 30X silicone immersion objective, with 1x zoom, binning 2x2, XY dimensions: 443.73 µm, thickness of z-stack at 11µm and z interval of 1µm. Images were randomly obtained from one section of every subject. To this end, the DG was first identified using a 10X dry objective in the DAPI channel. Next, stacks of images were obtained at randomly selected locations. Only the DAPI channel was visualized when selecting these locations. IHC, image acquisition, cell counts and image analyses were performed blind to the sex, age, PMD, and clinical diagnoses of the subjects. For the colocalization of the CR marker with other MC markers, confocal stacks of images and confocal tile scans were obtained with a Laser Scanning Confocal Microscope LSM900 coupled to an inverted Axio Observer Microscope (Zeiss).

Stereological Cell Counts

We performed stereological counts for each cell type, based on the marker expression, as well as the cell position and morphology. In the mouse DG, CR is expressed by MCs, interneurons and immature DGCs. In Tau^{VLW} mice, the number of immature neurons has already been reported to decrease, therefore we did not include the SGZ in our pictures, as we did not need to count that population of cells. We only acquired photos of the hilus and, as a result, we only had to discriminate between the 2 cell populations: MCs and interneurons. In the hilus, MCs have a larger size of soma and are characterized by multiple thorny excrescences, while interneurons are significantly smaller and do not display such rich dendritic structures. In the human DG, using the criteria described previously and in

Table 3, cell densities were estimated by unbiased stereology methods. Briefly, for the stacks of the mouse samples, only the hilus was present in the images, therefore the X and Y dimensions of the images were multiplied by the z-thickness of the stack to obtain the reference volume inside which the cells were counted. Physical dissector method modified for confocal microscopy was applied for CR^+ and $Dysbindin^+$ cell counts. Each positive cell was identified in the plane where it appears for the first time and this location is marked on every plane of the stack to avoid a single cell being counted multiple times. The formula that was used to calculate cell densities using the number of cells and the reference volume was: $\text{Cell density } (Number\ of\ cells/mm^3) = \frac{\text{Number of cells inside the reference volume}}{Reference\ Volume\ (mm^3)}$.

To calculate the total cell number of both the dorsal and the ventral area for each mouse, the average cell density (calculated from all the stacks obtained for each area) was multiplied with the volume of each region that was measured for that animal using Nissl staining.

For the stacks of images obtained from human samples, both part of the hilus and the dentate gyrus were present in the images, so depending on the population of cells that was being counted, the according area was drawn using the freehand selection tool of the Fiji software. Specifically, to count CR^+ immature neurons, the SGZ and the GCL were drawn. To count CR^+ mossy cells or interneurons, the hilus was drawn. This area was then multiplied by the z-thickness of the stack to calculate the reference volume inside which cells were counted. Cell densities were calculated using the same formula that was mentioned before. In this case, calculation of total cell number was not possible since we didn't have sections of the whole dentate gyrus for each human subject.

Statistical Analysis

Statistical analyses were conducted using GraphPad Prism 9 software (GraphPad.v.9.5.0 (730), 2022; GraphPad Software, LLC). The Kolmogorov-Smirnov normality test was used to check the normality of sample distribution (data distribution was considered to be normal when $p>0.05$). Atypical data were identified and extreme outlier values were eliminated when necessary. To compare between two experimental groups, a Student t-test was used in groups that showed normal sample distribution. For the groups where normality could not be assumed, a nonparametric test (Mann–Whitney U test) was performed. When the effects of more than one variable were analysed, a two-way ANOVA test was used. Fischer LSD post hoc analysis was used to compare the differences between individual groups. In those cases, asterisks on the graphs represent the results of post-hoc inter-subject multiple comparison tests. All graphs represent mean values ± SEM. A 95% confidence interval was used for all statistical comparisons.

Results

Mouse experiments

Dentate Gyrus Volume

Using Nissl staining, we compared the volume of the DG of Tau^{VLW} and control mice (*Figure 5*). Expression of the mutated human Tau caused a statistically significant difference in this parameter. In the Tau^{VLW} animals, there was a decrease in the volume of both the dorsal ($mean_{C57} = 0.45mm^3 \pm 0.0195$, $mean_{TauVLW} = 0.34mm^3 \pm 0.0195$, $p<0.0001$) (*Figure 6: B*) and the ventral ($mean_{C57} = 0.10mm^3 \pm 0.009$, $mean_{TauVLW} = 0.08mm^3 \pm 0.009$, $p = 0.046$) DG (*Figure 6: A*). This result is in agreement with a previous study from the lab, where a reduction in the ventral DG volume and in the number of mature DGCs in the same region was also shown.[35] Moreover, a statistically significant reduction of the total DG volume was observed in Tau^{VLW} mice ($mean_{C57} = 0.55mm^3 \pm 0.022$, $mean_{TauVLW} = 0.42mm^3 \pm 0.022$, $p<0.0001$) (*Figure 6: C*). Details of the statistical tests are included in *Table 4*, in the statistics annex.

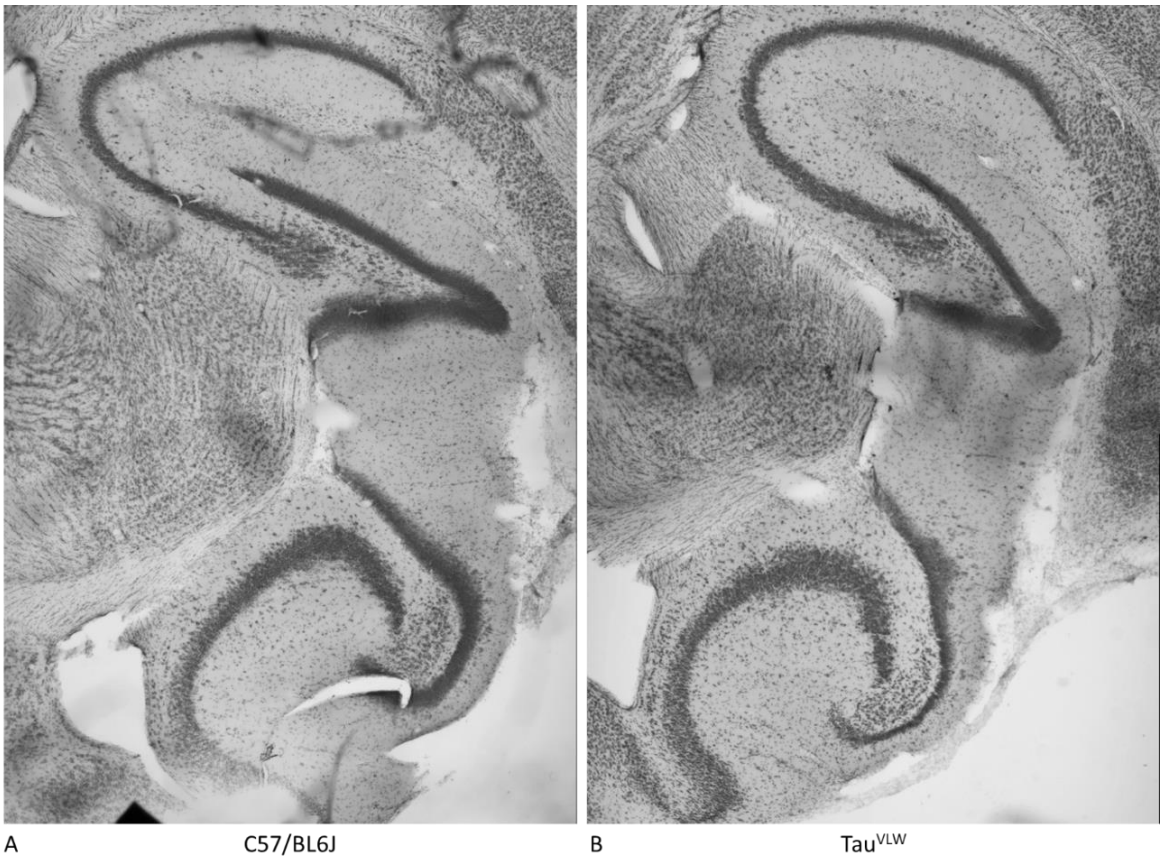

Figure 5: DG of control and Tau^{VLW} mice. Representative pictures of NISSL stained DG from A:C57 control mice and B: Tau^{VLW} mice.

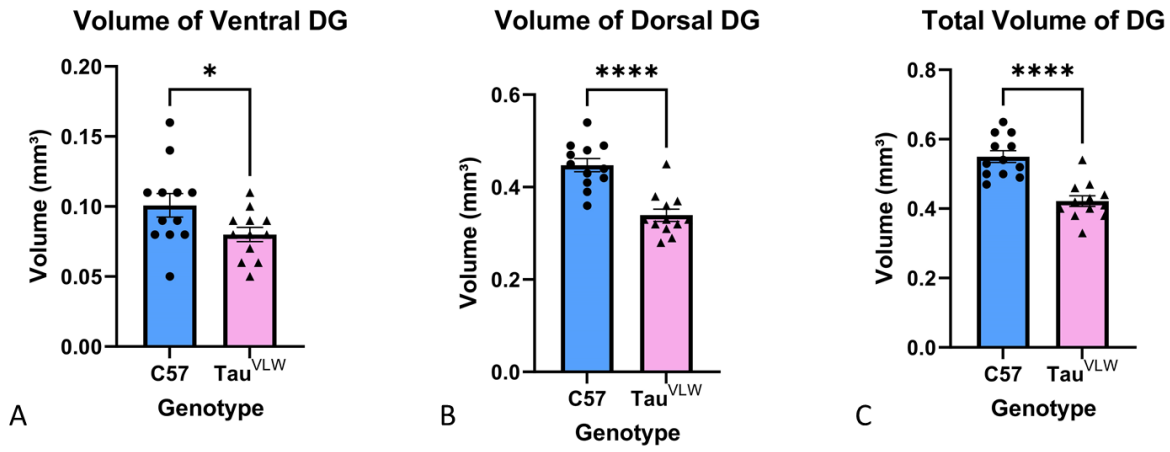

Figure 6: Volume of DG in control and Tau^{VLW} mice. A: Volume of the ventral DG of C57 and Tau^{VLW} mice. The latter display a decreased ventral DG volume. B: Volume of the dorsal DG of C57 and Tau^{VLW} mice. The latter display a decreased dorsal DG volume. C: Total DG volume of C57 and Tau^{VLW} mice. Tau^{VLW} mice display decreased total DG volume.

Number of CR^{+} and Dysbindin^{+} Cells

We performed double IHC to compare the number of MCs between the two genotypes. In the mouse hilus, CR is expressed in MCs and interneurons. Therefore, we counted the number of each cell type separately, based on the cell position and morphology, as mentioned earlier. All the Dysbindin-expressing cells in the mouse DG are MCs (*Figure 7*). Total cell number was calculated and two-way ANOVA was performed to compare the following factors: genotype (Tau^{VLW} vs C57/BL6J), area (dorsal vs ventral), as well as their interaction, followed by post-hoc comparisons to compare the differences between the individual groups.

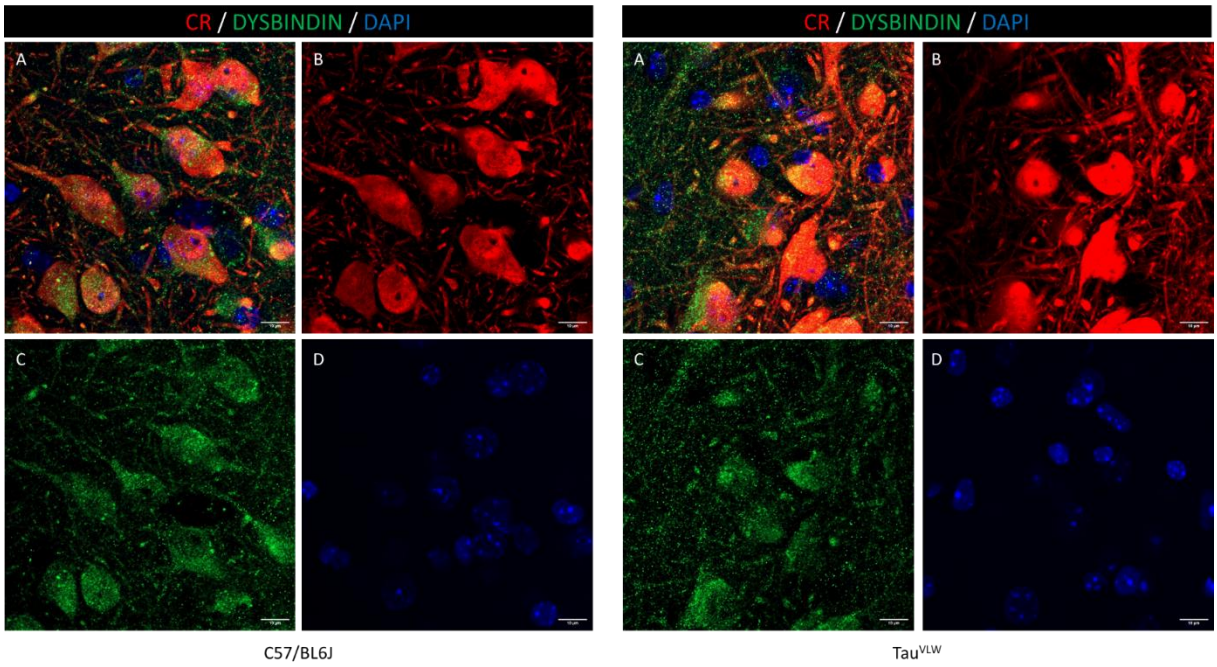

Figure 7: Hilus of control and Tau^{VLW} mice. Representative pictures of double IHC experiments on control (left) and Tau^{VLW} (right) mice. CR (B-red), Dysbindin (C-green), DAPI (D-blue) and merge (A) show that MCs express CR and Dysbindin in the mouse DG. Picture

For the CR^+ MCs, the two-way ANOVA revealed that the interaction between genotype and area was not significant (F=0.5, p=0.485). The DG area (dorsal or ventral) was also not significant (F=3.8, p=0.06). The genotype however did have a statistically significant effect on the variance (F=7.13, p=0.013). The post-hoc comparisons revealed a statistically significant decrease in the number of CR^+ MCs in the ventral part of the hilus of Tau^{VLW} mice compared to the control mice DG ($mean_{C57}$ = 18931 ± 1814 cells, $mean_{TauVLW}$ = 9819 ± 1814 cells, p = 0.025). No statistically significant changes were found in the remaining comparisons (Dorsal C57 vs Dorsal Tau^{VLW}, Dorsal C57 vs Ventral C57, Dorsal Tau^{VLW} vs Ventral Tau^{VLW}) (*Figure 8: A*).

Similarly, for the $Dysbindin^+$ MCs, the two-way ANOVA showed that interaction between genotype and area was not significant (F=0.17, p=0.682). The DG area was also not significant (F=0.57, p=0.457). The genotype did have a statistically significant effect on the variance (F=8.58, p=0.007). The post-hoc comparisons showed a statistically significant decrease in the ventral part of the hilus of the Tau^{VLW} compared to the C57/BL6J mice ($mean_{C57}$ = 18681 ± 3749 cells, $mean_{TauVLW}$ = 9819 ± 3749 cells, p = 0.027). No statistically significant changes were found in the remaining comparisons (Dorsal C57 vs Dorsal Tau^{VLW}, Dorsal C57 vs Ventral C57, Dorsal Tau^{VLW} vs Ventral Tau^{VLW}) (*Figure 8: B*).

The two-way ANOVA for the double labelled MCs (CR^+/$Dysbindin^+$), revealed that the interaction between genotype and area was not significant (F=0.52, p=0.479). The DG area was also not significant (F=4.01, p=0.057). The genotype did have a statistically significant effect on the variance (F=6.94, p=0.015). The post-hoc comparisons showed a statistically significant decrease in the ventral region in Tau^{VLW} compared to the C57/BL6J mice ($mean_{C57}$ = 18681 ± 3750 cells, $mean_{TauVLW}$ = 9791± 3750 cells, p = 0.026). No statistically significant changes were found in the remaining comparisons (Dorsal C57 vs Dorsal Tau^{VLW}, Dorsal C57 vs Ventral C57, Dorsal Tau^{VLW} vs Ventral Tau^{VLW}) (*Figure 8: C*).

Concerning the CR^+ interneurons, the two-way ANOVA revealed that interaction between genotype and area was not significant (F=0.58, p=0.453). The genotype was also not significant (F=3.21, p=0.087). The DG area did have a statistically significant effect on the variance (F=6.05, p=0.022). The post-hoc comparisons showed a statistically significant decrease in the ventral part of the Tau^{VLW} DG compared to the dorsal part in the same genotype ($mean_{Dorsal}$ = 1528 ± 487.7 cells, $mean_{Ventral}$ = 417 ± 487.7 cells, p = 0.033). No statistically significant changes were found in the remaining comparisons (Dorsal C57 vs Dorsal Tau^{VLW}, Ventral C57 vs Ventral Tau^{VLW}, Dorsal C57 vs Ventral C57) (*Figure 8: D*). Details of the statistical tests are included in *Table 5*, in the statistics annex.

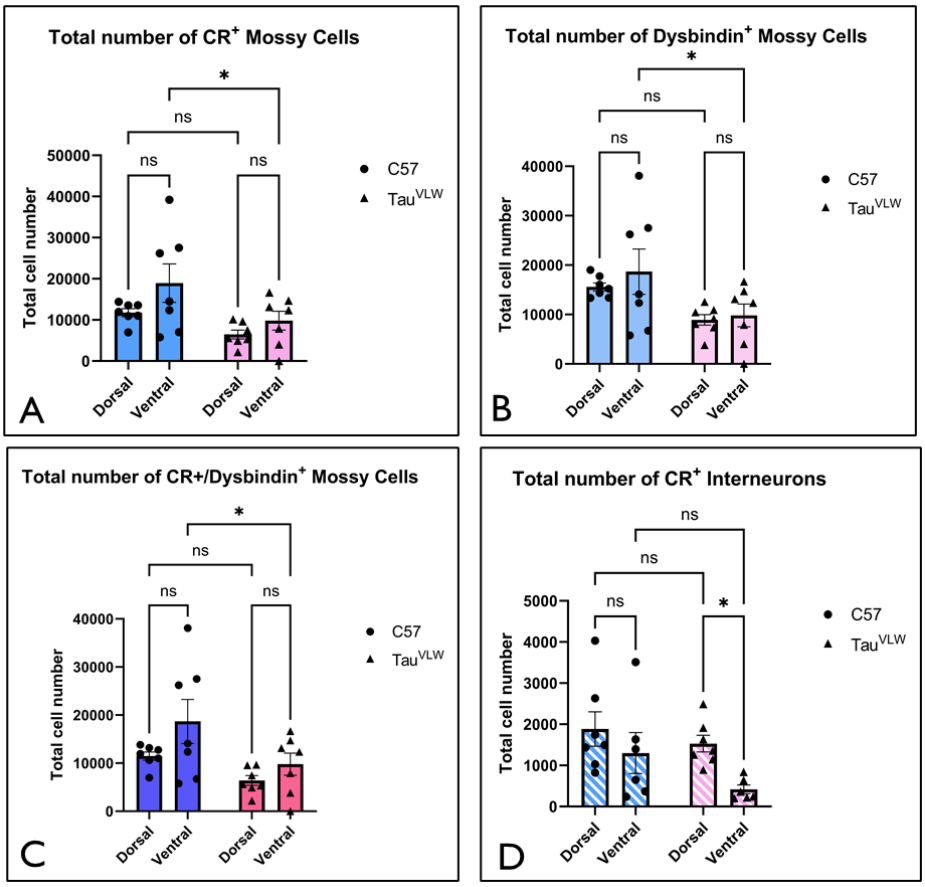

Figure 8: MC numbers in control and Tau^{VLW} mice. A: CR$^+$ MC number in the dorsal and ventral DG of C57 and Tau^{VLW} mice. Tau^{VLW} mice display a decrease in the number of CR$^+$ MCs in the ventral DG. B: Dysbindin$^+$ MC number in the dorsal and ventral DG of C57 and Tau^{VLW} mice. Tau^{VLW} mice display a decreased number of Dysbindin$^+$ MCs in the ventral DG. C: Double labelled MC number in the dorsal and ventral DG of C57 and Tau^{VLW} mice. Tau^{VLW} mice display a decrease in the number of double labelled MCs in the ventral DG. D: Number of CR$^+$ interneurons in the dorsal and ventral DG of C57 and Tau^{VLW} mice. In the Tau^{VLW} group, there is a decrease in the number of CR$^+$ interneurons in the ventral compared to the dorsal DG.

CR Expression Gradient in the Latero-medial Axis of the Mouse Dorsal DG

We observed that, in the most lateral parts of the DG, all MCs were double-labelled in both the dorsal and ventral areas. However, within the dorsal region, a notable shift manifested as we progressed medially: while all MCs continued to express Dysbindin, only a few of them demonstrated immunoreactivity for CR (*Figure 9*). Consequently, we performed a quantitative analysis, aiming to compare the proportion of Dysbindin$^+$ MCs co-expressing CR across various positions along the latero-medial axis of the hippocampus.

As it is shown in *Figure 10: A*, in the utmost lateral positions, the CR-to-Dysbindin ratio was 1, and this ratio progressively decreased with proximity to the midline. This pattern held consistent in both control and Tau^{VLW} mice. Subsequently, we statistically explored these variations. Given the inherent non-uniformity in brain sectioning and the stochastic nature of series selection, ensuring precise anatomical alignment between different mice was unfeasible. As a result, we decided to group the ratios derived from the two most lateral, two middle and two most medial slices within each mouse, and perform the comparison between those three groups.

A two-way ANOVA was performed to explore the factors: genotype and position on the latero-medial axis, as well as the interaction between them. The analysis revealed that the interaction between the two factors was not significant (F=0.49, p=0.6165). The effect of the genotype was also not significant (F=1.58, p=0.2165). The position on the latero-medial axis did have a statistically significant effect on the variance (F=47.89, p<0.0001). The post-hoc comparisons showed a statistically significant decrease in the proportion of Dysbindin^{+} MCs expressing CR when comparing the most lateral slices with the middle ones (C57: p=0.0441, Tau^{VLW}: p=0.0069), as well as, when comparing the middle slices with the most medial ones (C57: p=0.0003, Tau^{VLW}: p<0.0001), in both the C57/BL6J and the Tau^{VLW} group. No statistically significant changes were found when comparing between genotype (*Figure 10: B*). Details of the statistical tests are included in *Table 6*, in the statistics annex.

This observed gradient in CR expression along the latero-medial axis in the dorsal DG potentially sheds light on the prevailing literature indicating limited CR expression in dorsal MCs. This may be attributed to the prevalent use of coronal sections, in which the dorsal part of the DG is more prominent in the positions closer to the midline. Consequently, we support that dorsal MCs do indeed exhibit CR expression, and this expression decreases as we progress from the lateral aspects of the murine brain towards the midline.

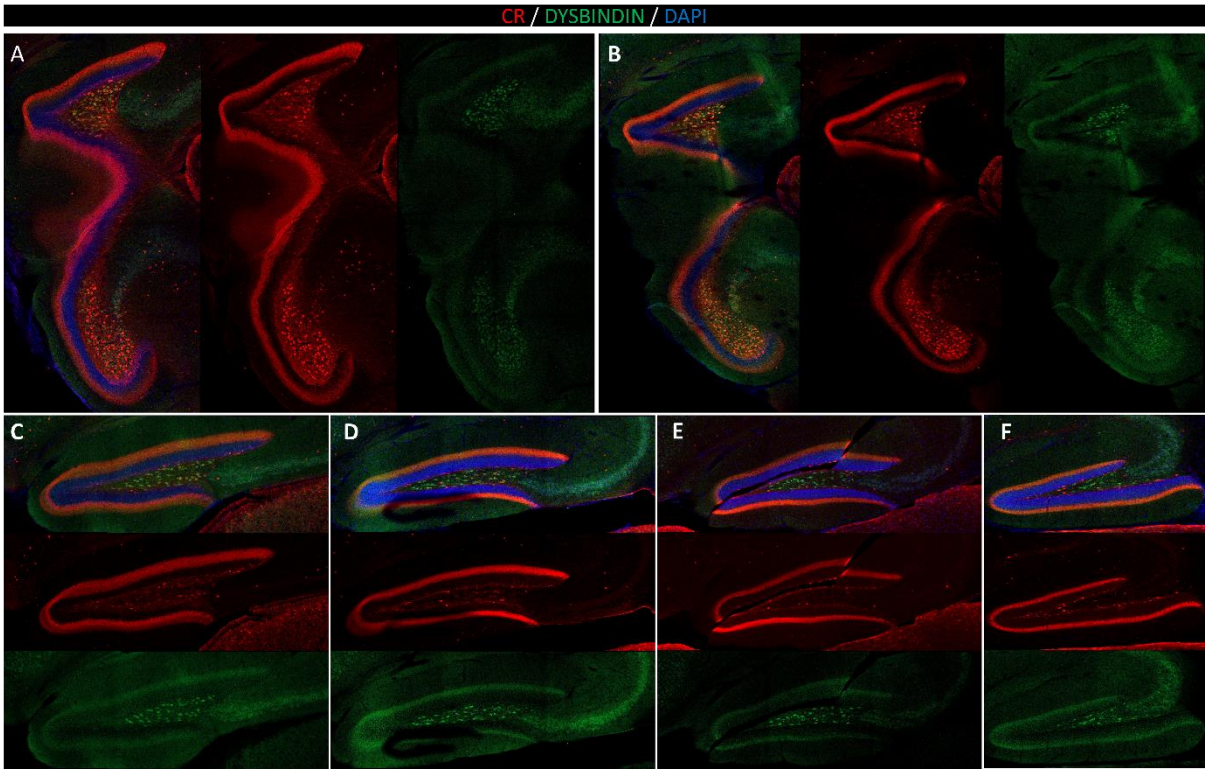

Figure 9: DG of a C57 mouse after double IHC with CR and Dysbindin. Representative tile scans across the latero-medial axis, starting from the most lateral points (A) and continuing closer to the midline (F). In the pictures of the most lateral parts, MC of the dorsal DG express both CR and Dysbindin, but CR expression is lost in the most medial slices.

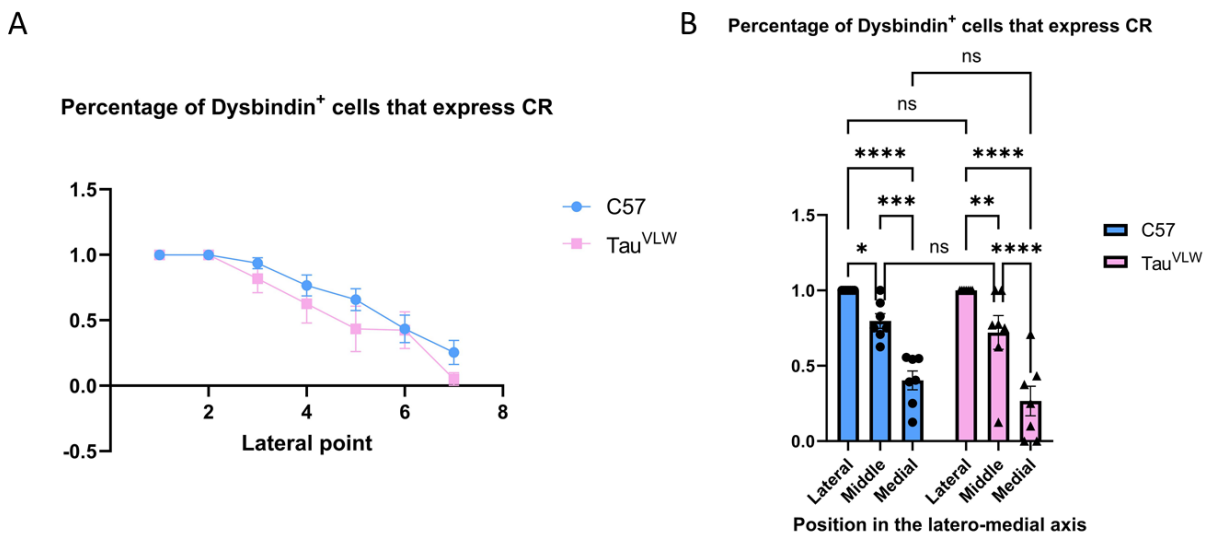

Figure 10: Graphs representing the CR expression gradient across the latero-medial axis. A: Graph showing the ratio of Dysbindin$^+$ cells that also express CR in the dorsal DG in control (blue) and Tau^{VLW} (pink) mice. B: Bargraph showing the grouped lateral, middle and medial slices. The decrease in the percentage of Dysbindin$^+$ cells that also express CR is statistically significant between the three groups.

Human experiments

DCX

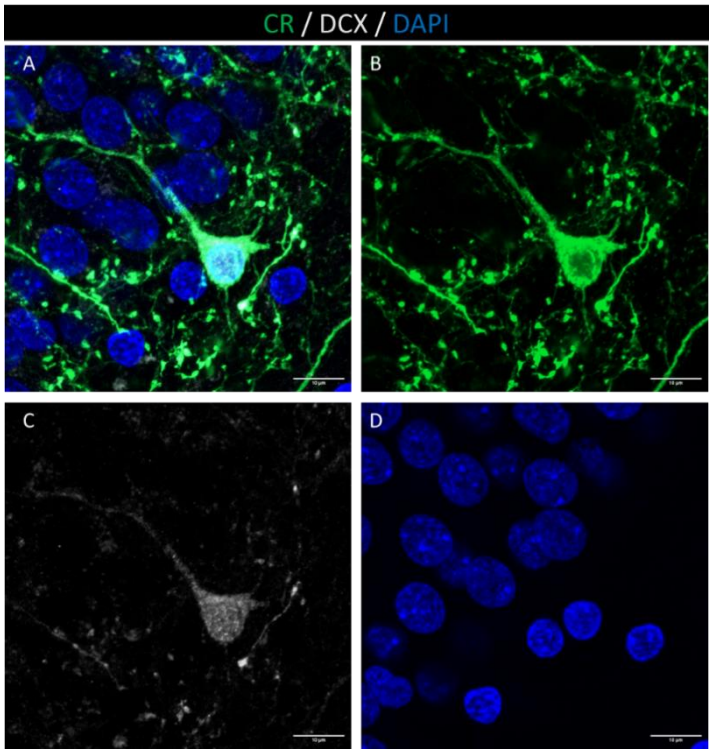

Figure11: High-magnification image of the SGZ of a healthy human subject stained with CR and DCX. One DCX+/CR+ immature neuron is observed in the SGZ, with its typical morphology. A: Merge, B: CR, C: DCX and D: DAPI channels are showed. Scalebar: 10µm

We employed DCX/CR double IHC to discriminate between CR$^+$ immature DGCs and interneurons. In *Figure 11*, an image from a healthy control human subject, stained with CR and DCX, is shown. We observed DCX$^+$/CR$^+$ immature DGCs in the SGZ. These cells had small size, and a characteristic

morphology with the apical dendrite extending toward the ML. We also spotted CR^+ interneurons, located in the hilus, having a small size and the anticipated absence of DCX staining (*Figure 12*), consistent with established expectations for such cell types.

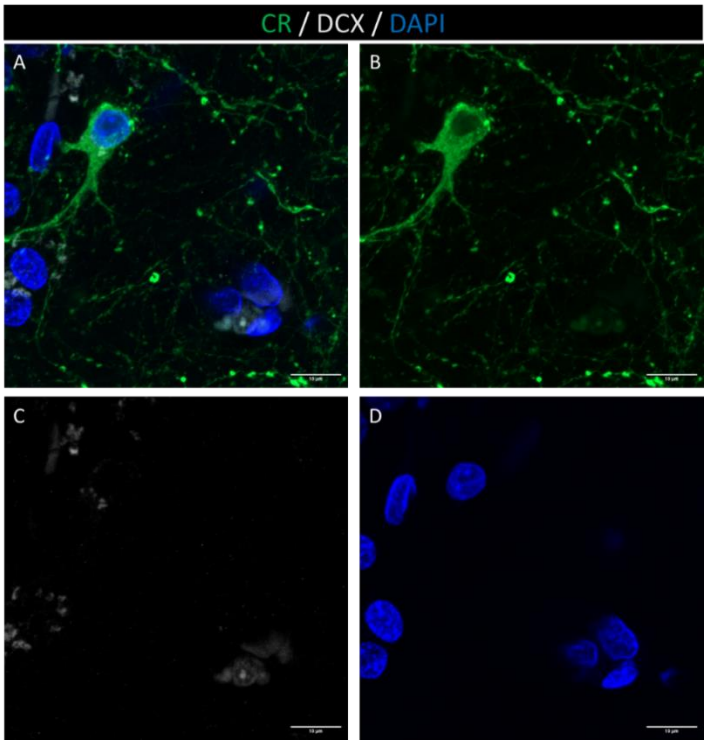

Figure12: High-magnification image of the hilus of a healthy human subject stained with CR and DCX. One DCX-/CR+ interneuron is observed. A: Merge, B: CR, C: DCX and D: DAPI channels are showed. Scalebar: 10μm

Density of CR^+ cells

According to the prevailing literature, in the human DG, CR is expressed by immature GC and some hilar interneurons, but not by MC.[114,123] However, while observing our human sections in the microscope after staining them with CR, we noticed the existence of some CR-immunoreactive cells that fit the description of MCs (*Figure 13*). Those cells are located in the hilus, have a large soma (~30μm) and display extensive dendritic structures. We also noted that they showed a low signal in the DAPI channel, compared to their surrounding cells. Based on these characteristics, we discriminated among those ‘’potential’’ MCs, hilar interneurons and immature DGCs that express CR. CR+ hilar interneurons are also located in the hilus but are much smaller in size than MCs and don’t have extensive dendritic branches. Immature DGCs are located in the SGZ and are also smaller in size, show a very defined oval shape, and usually have a vertical orientation with their apical dendrite towards the ML. In *Table 3* we have summarized the criteria used to discriminate between the different cell types in the human DG.

Table 3: Criteria used to differentiate between CR⁺ neurons in the human DG.

	CR⁺ MCs	**CR⁺ IMMATURE DGCs**	**CR⁺ INTERNEURONS**
Location	Hilus	SGZ	Hilus
Size	Big (~30µm)	Small (~10µm)	Small (~10µm)
Prominent branches	Yes	No (apical dendrite towards the ML)	No

The comparison of MC density between control human subjects and FTD patients showed no statistically significant difference ($mean_{Control}$ = 1158 ± 242 cells/mm^3, $mean_{FTD}$ = 1192 ± 242 cells/mm^3, p = 0.8913) (*Figure 14: A*). However, the comparison of CR⁺ immature neurons density between control human subjects and FTD patients revealed a statistically significant decrease in the FTD group ($mean_{Control}$ = 2451 ± 498.5 cells/mm^3, $mean_{FTD}$ = 779 ± 498.5 cells/mm^3, p = 0.0043) (*Figure 14: B*). This is consistent with the previously described decreased neurogenesis in human subjects of FTD by our group.[128] Additionally, the comparison of CR⁺ interneurons density between control human subjects and FTD patients revealed a statistically significant decrease in FTD patients ($mean_{Control}$ = 4064 ± 688.5 cells/mm^3, $mean_{FTD}$ = 2497 ± 688.5 cells/mm^3, p = 0.0370) (*Figure 14: C*). Details of the statistical tests are included in *Table 7*, in the statistics annex.

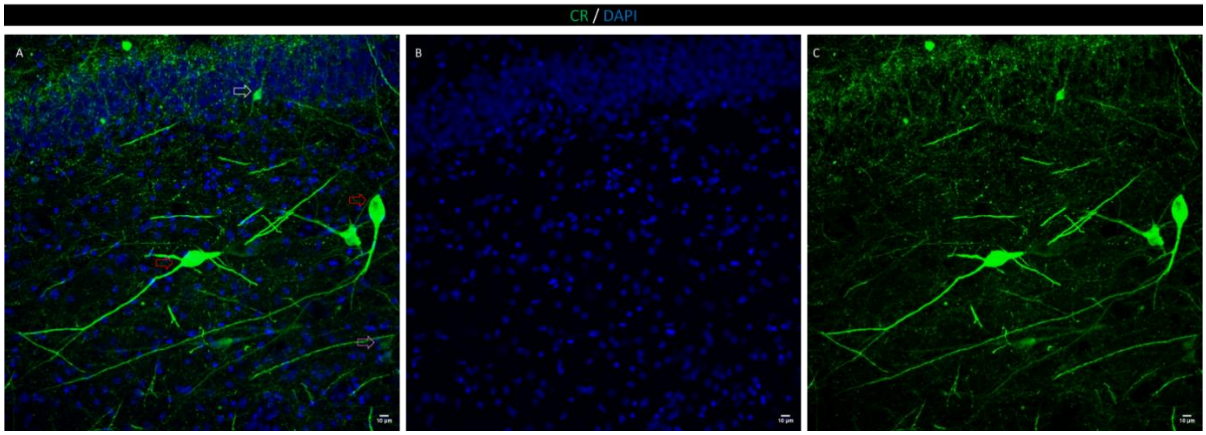

Figure 11: CR IHC in human DG. Representative picture of merge (A), DAPI (B) and CR (C) staining in a healthy control. Red arrows show CR+ MC, white arrow shows CR+ immature GC and pink arrow shows CR+ interneuron. Scalebar: 10µm

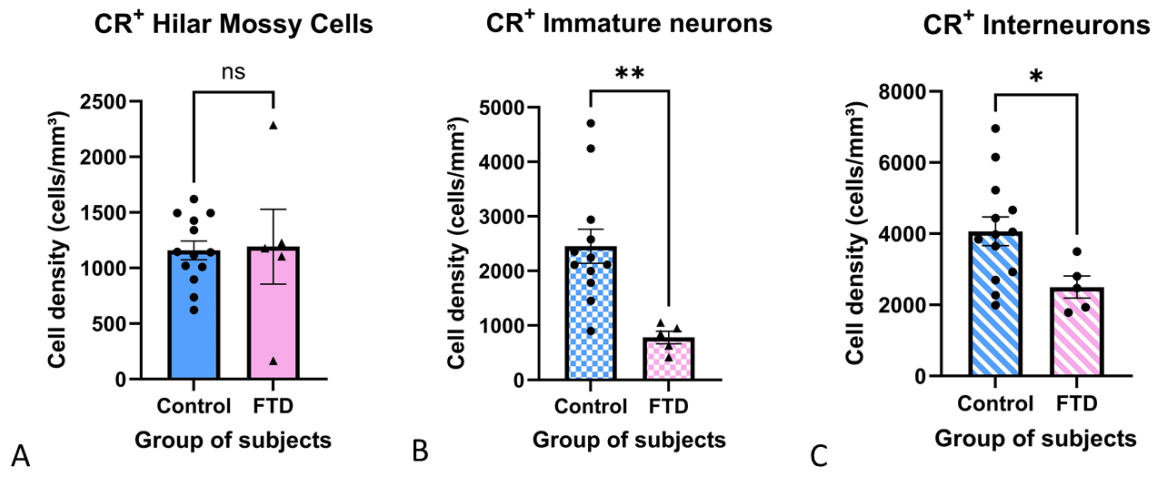

Figure 12: CR⁺ MCs, Immature neurons and Interneurons in patients with FTD and healthy control subjects. A: CR⁺ MC density in the DG of FTD patients and healthy control subjects. No significant changes were detected. B: CR⁺ Density of immature DGCs in the DG of FTD patients and healthy control subjects, showing a reduction in FTD patients. C: CR⁺ Interneuron density in the DG of FTD patients and healthy control subjects, showing a decrease in the former.

Human Mossy Cell Markers

Following the stereological quantification analysis conducted on the acquired stacks of images, we conducted a series of qualitative experiments to validate some potential MC markers in human samples. Our objective was to ascertain whether the CR+ MCs exhibited the presence of markers that are considered more typical for MCs. This was particularly challenging due to the scarcity of studies addressing this cell type in human tissue. To this end, we selected CR, Dysbindin, CART, and D2R as our primary markers of interest, given the extensive literature that exists for murine models. Additionally, we employed DCX to furtherly confirm the identity of immature neurons and interneurons.

Dysbindin

Upon conducting double IHC for Dysbindin and CR, we observed that Dysbindin staining patterns closely resembled those that we previously documented in mice. This similarity stemmed from a substantial proportion of hilar cells exhibiting Dysbindin immunoreactivity (*Figure 15*). Given that MC constitute approximately 30% of hilar neurons, this staining pattern was in closer alignment with our expectations compared to the CR images, where fewer cells were stained. However, a notable observation emerged: a subset of Dysbindin-expressing MC also exhibited CR immunoreactivity (*Figure 16*). Based on these findings, we propose that the majority, if not all, of human MCs express Dysbindin, while only some of these cells show CR immunoreactivity. These observations suggest the presence of distinct subpopulations of MCs within the human hippocampus, potentially indicating functional heterogeneity. Furthermore, we were able to identify CR⁺ immature DGCs and CR⁺ interneurons that did not express Dysbindin, which further support our previous criteria (*Figure 17*).

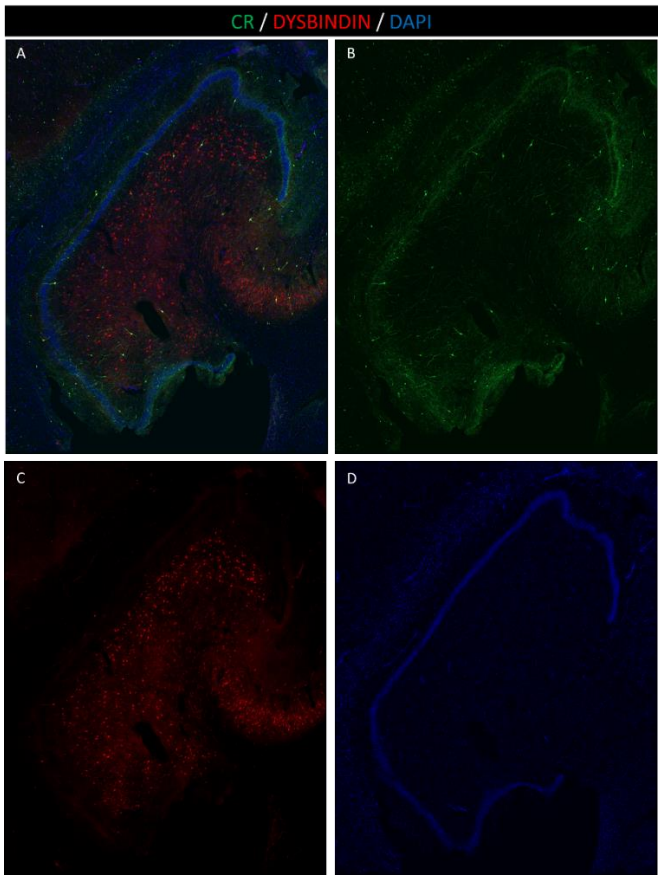

Figure 13: DG of healthy control human subject stained with CR and Dysbindin. A: Merge, B: CR, C: Dysbindin and D: DAPI channels are showed.

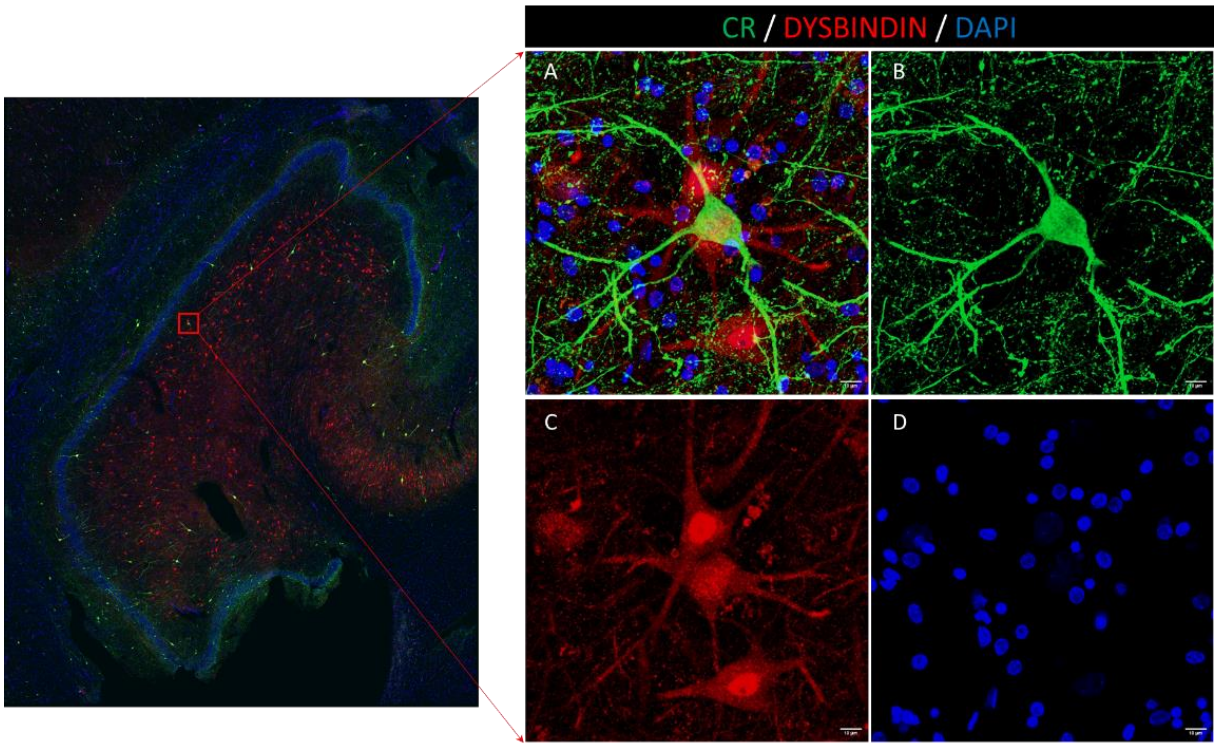

Figure 14: High-magnification image of the hilus of a healthy control human subject stained with CR and Dysbindin. Several Dysbindin+ MC are observed, as well as a Dysbindin+/CR+ MC. A: Merge, B: CR, C: Dysbindin and D: DAPI channels are showed. Scalebar: 10μm

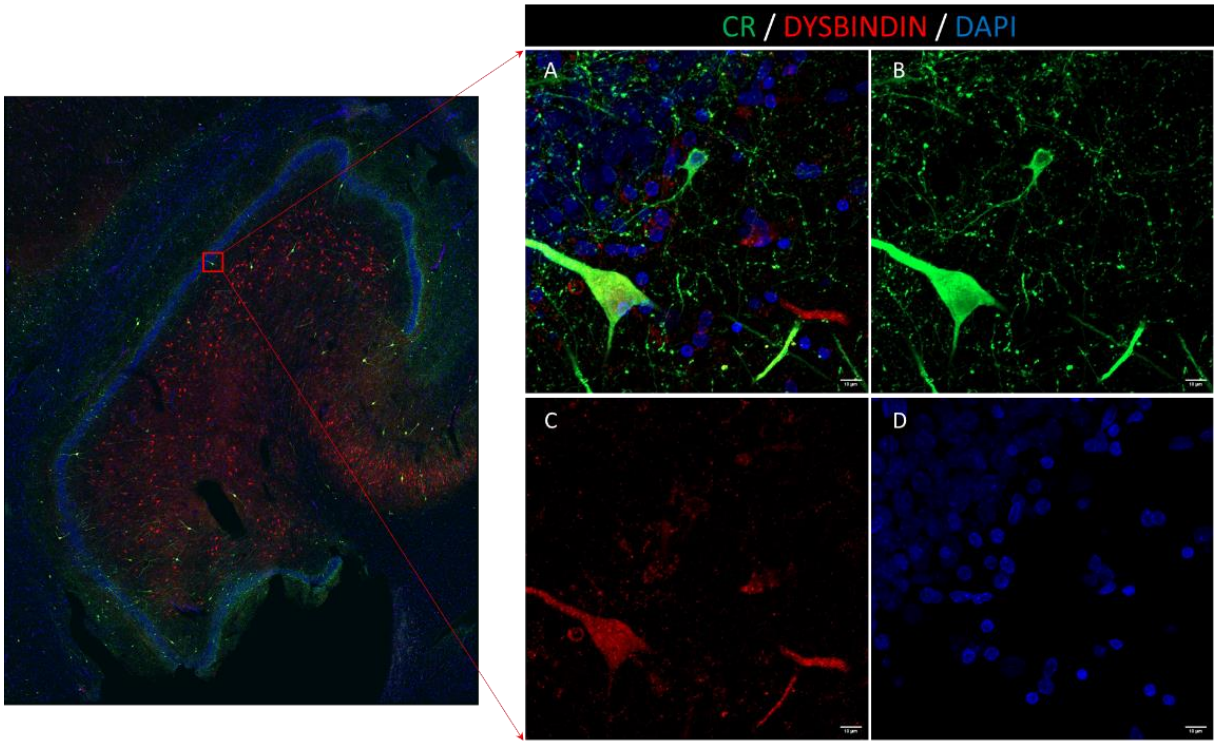

Figure 15: High-magnification image of the SGZ of a healthy control human subject stained with CR and Dysbindin. One Dysbindin$^+$/CR$^+$ MC, as well as a CR$^+$/Dysbindin$^-$ immature neuron can be observed. A: Merge, B: CR, C: Dysbindin and D: DAPI channels are showed. Scalebar: 10μm

CART

In the context of the CART/CR double IHC, the acquired images exhibited similarity between the two markers with respect to the number of MC displaying immunoreactivity. We observed that CART labelled a subset of MCs, albeit not all, when compared to the staining patterns observed in the dysbindin images (*Figure 18*). It is important to note, however, that the quality of the CART antibody signal is suboptimal. It is, of course, possible that CART may label only a subpopulation of MCs, like our previously suggested scenario for CR. Our observations revealed the presence of MC that were double-labelled, implying concurrent expression of CART and CR. However, we also noted the existence of CART$^+$/CR$^-$ and CART$^-$/CR$^+$ MC subpopulations (*Figure 19*). Additionally, we showed the presence of CR$^+$ immature DGCs, as well as CR$^+$ interneurons, that lacked CART staining (*Figure 20*). These observations strengthen our previous cell discrimination criteria in the human DG.

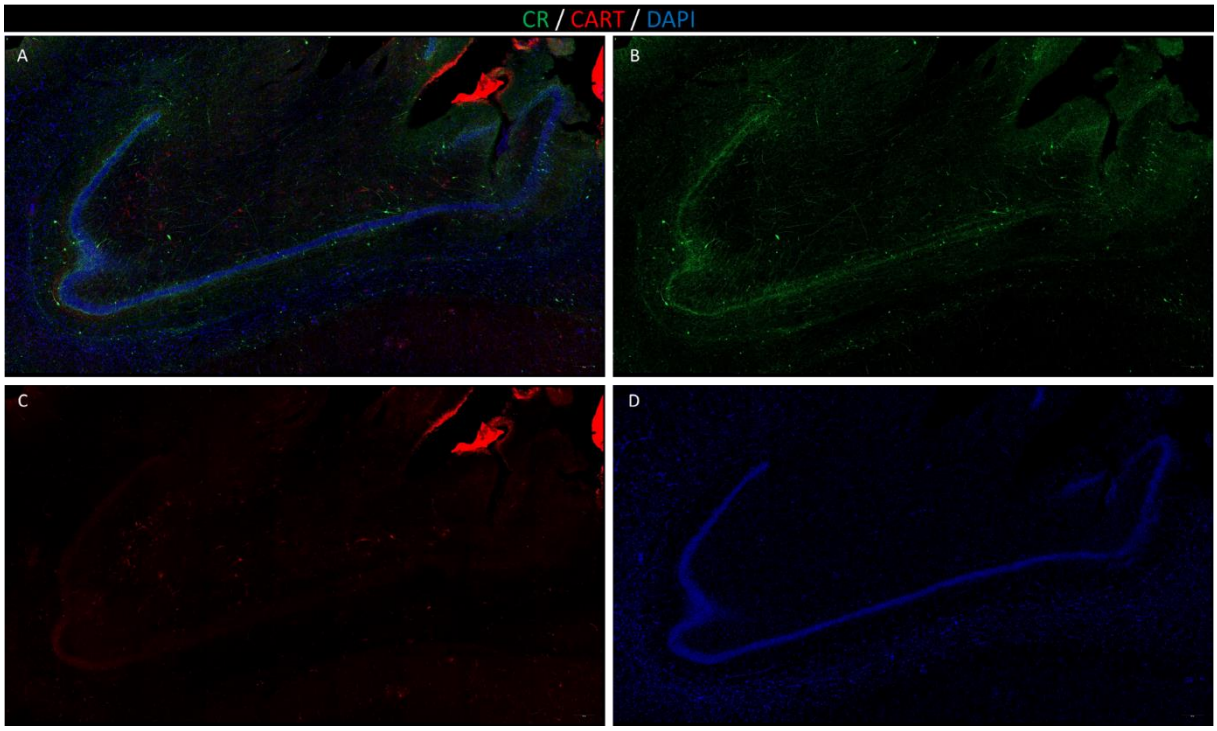

Figure 16: DG of healthy human subject stained with CR and CART. A: Merge, B: CR, C: CART and D: DAPI channels are showed.

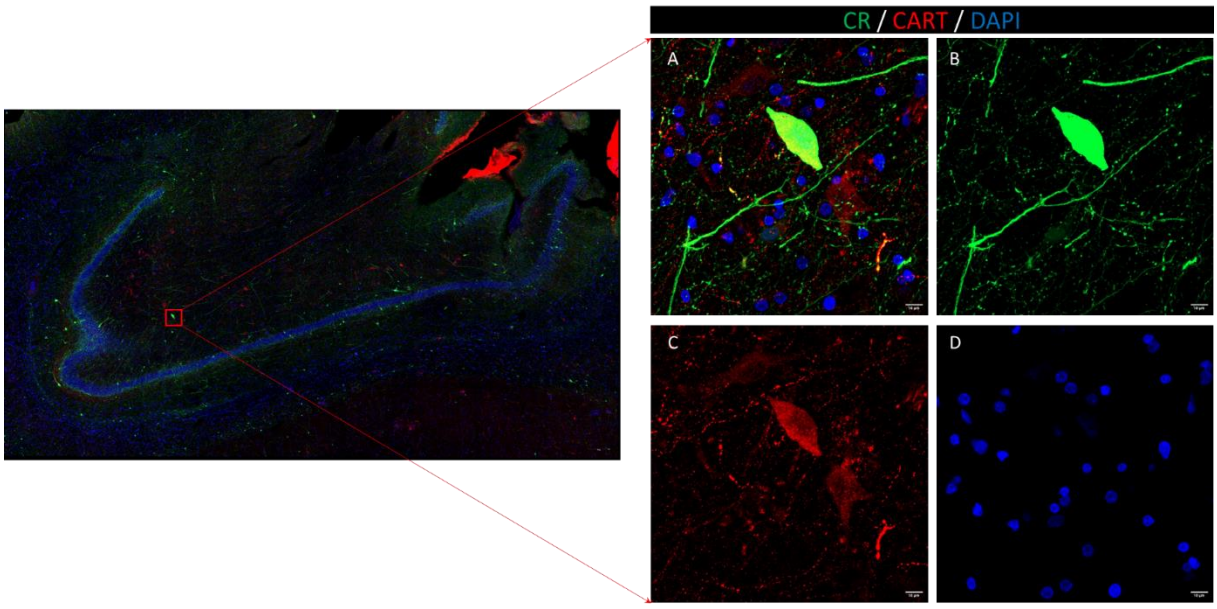

Figure 17: High-magnification image of the hilus of a healthy human subject stained with CR and CART. Few CART+ MC are observed, as well as a CART+/CR+ MC. A: Merge, B: CR, C: CART and D: DAPI channels are showed. Scalebar: 10µm

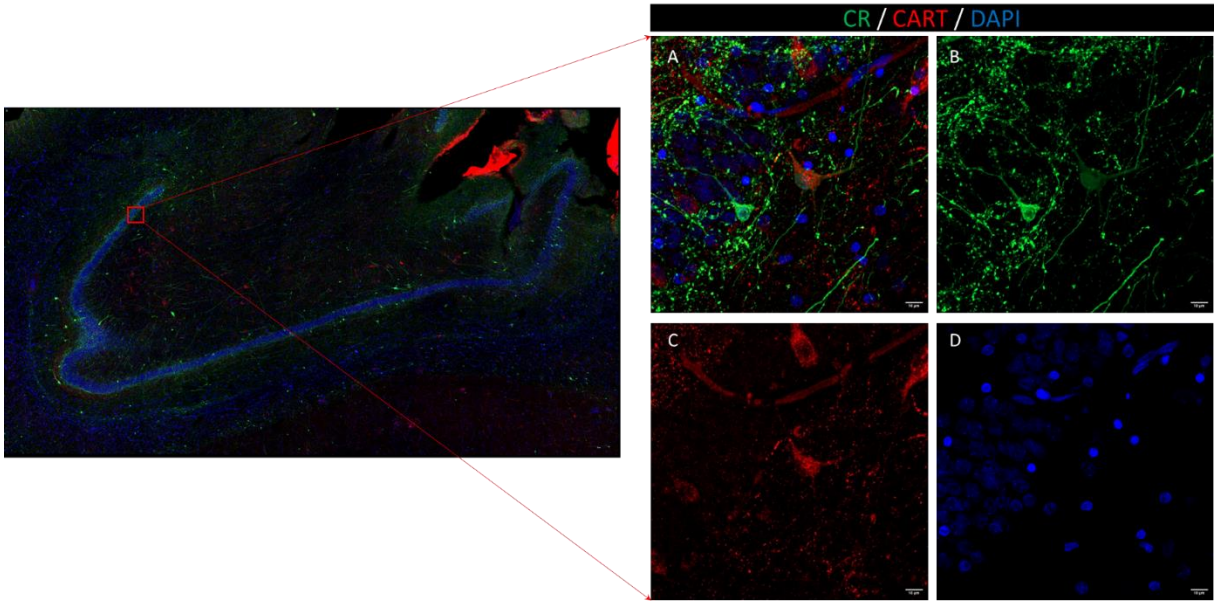

Figure 18: High-magnification image of the SGZ of a healthy human subject stained with CR and CART. A CART+/CR+ MC is observed, as well as a CART-/CR+ immature neuron and a CART+/CR- GC. A: Merge, B: CR, C: CART and D: DAPI channels are showed. Scalebar: 10μm

D2R

For the D2R/CR double IHC, the acquired images exhibited a resemblance to the CART and CR images in terms of the number of labelled MCs. We should note, again, the quality of the D2R antibody is not the optimal, therefore, no concrete conclusions can be made, based on these pictures (*Figure 21*). Our suggestion is that only a subpopulation of MCs expresses D2R, which mirrors our previous propositions for CART and CR. Furthermore, we did observe the presence of MCs that were double-labeled, signifying concurrent expression of D2R and CR (*Figure 22*). Nevertheless, we also identified $D2R^{+}/CR^{-}$ and $D2R^{-}/CR^{+}$ MCs. Additionally, we found CR^{+} immature DGCs, as well as CR^{+} interneurons, that lacked D2R staining (*Figures 22, 23*). These observations reinforce the robustness of our criteria for discerning and characterizing different CR^{+} cell types. Furthermore, we noted the presence of D2R staining in certain GCs (*Figure 23*), which aligns with the suggestion that the GCL receives dopaminergic innervation.[129,130]

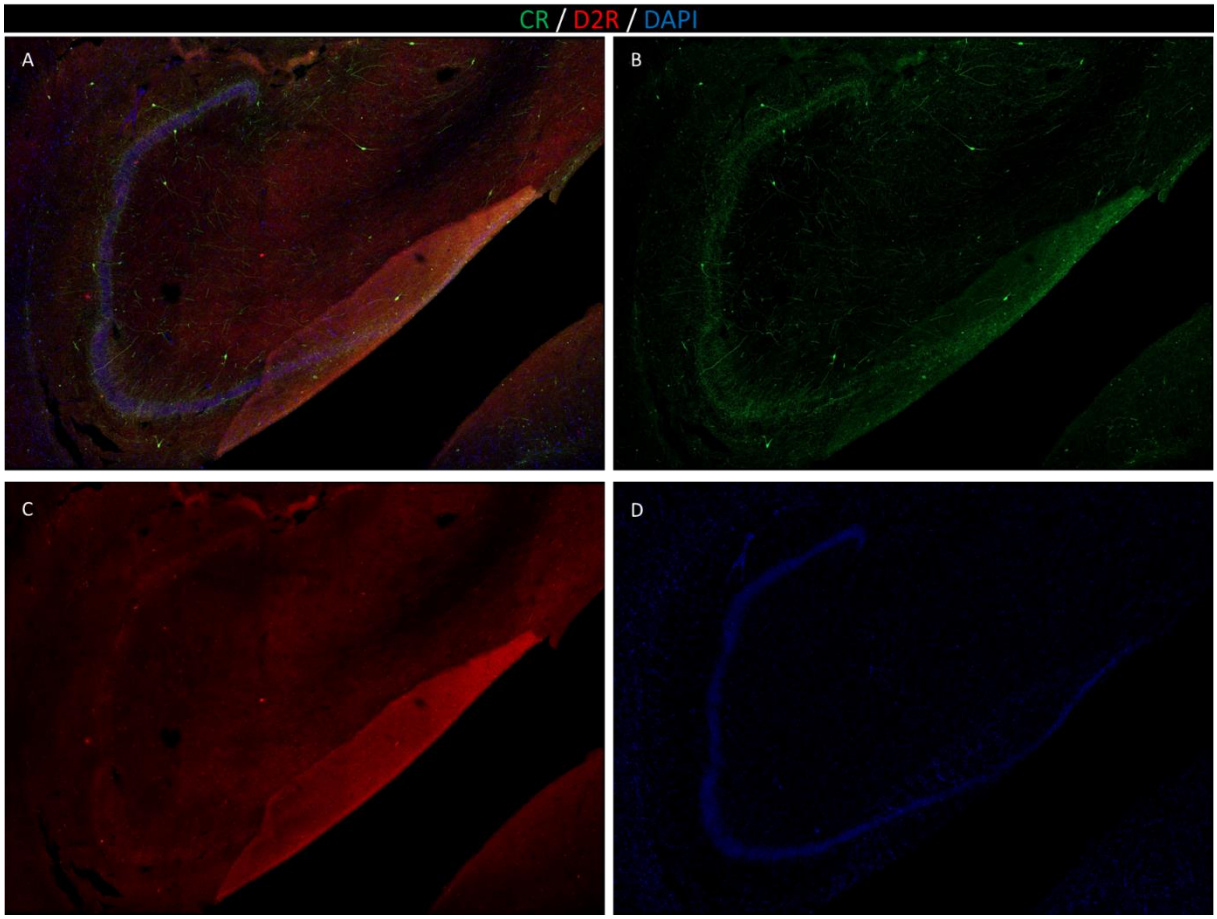

Figure 19:DG of healthy human subject stained with CR and D2R. A: Merge, B: CR, C: D2R and D: DAPI channels are showed.

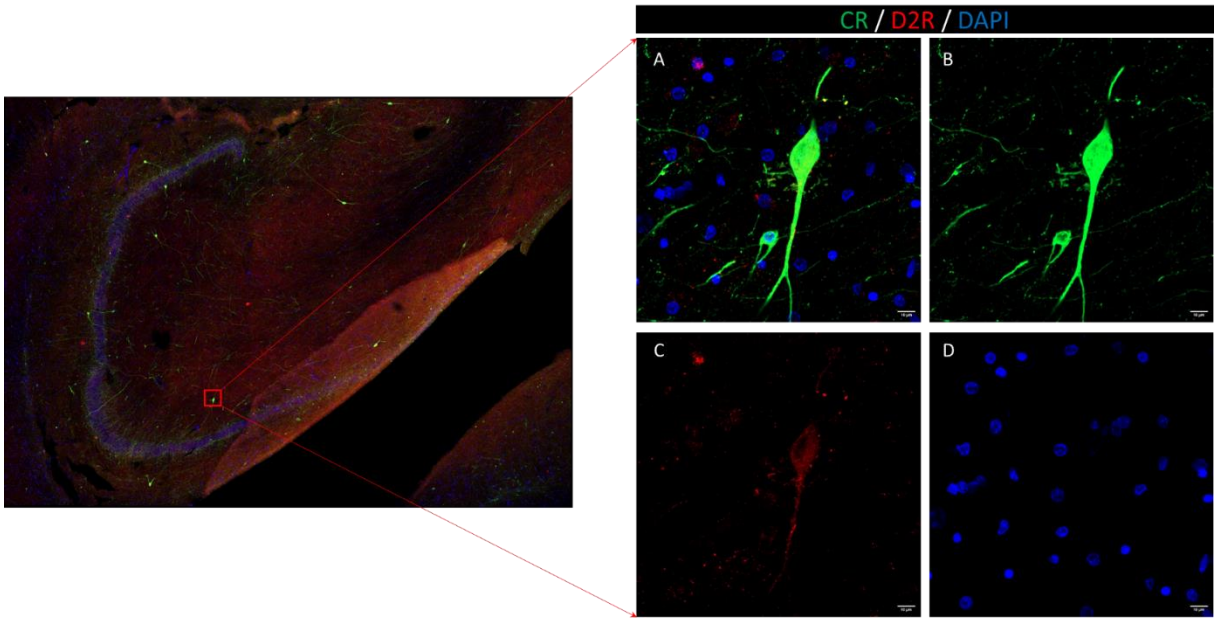

Figure 20: High-magnification image of the hilus of a healthy human subject stained with CR and D2R. One D2R+/CR+ MC is observed, as well as a D2R-/CR+ interneuron. A: Merge, B: CR, C: D2R and D: DAPI channels are showed. Scalebar: 10μm

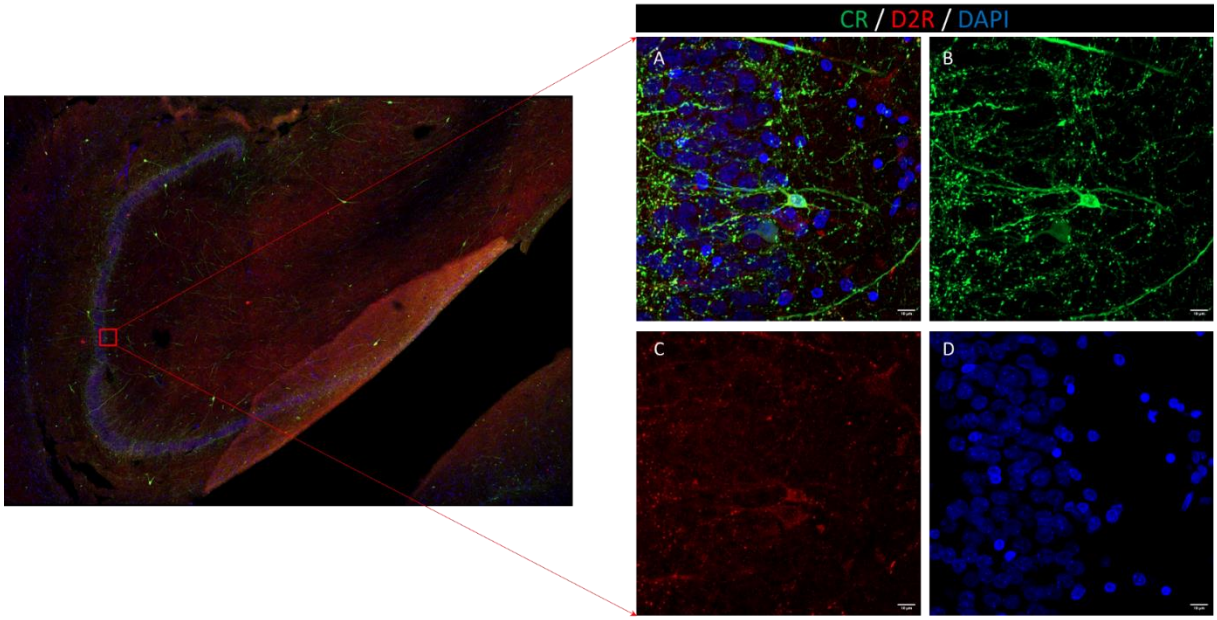

Figure 21: High-magnification image of the SGZ of a healthy human subject stained with CR and D2R. One D2R+/CR+ immature neuron is observed, as well as a D2R+/CR- immature neuron. A: Merge, B: CR, C: D2R and D: DAPI channels are showed. Scalebar: 10μm

Discussion

In this study, we focused on hilar MCs and their potential changes during FTD. We used brain tissue from both an FTDP-17 mouse model and patients with this disorder. First, we measured the volume of the DG and we found that both the dorsal and the ventral part of this region is decreased in Tau^{VLW} mice, compared to their wild-type counterparts. The reduction of the ventral DG volume has been reported before, along with a decrease in neural precursor cell proliferation and increase of cell death in that area in this mouse model.[35] We also found a statistically significant decrease in the number of CR^{+}, $Dysbindin^{+}$ and double labelled MCs in the ventral part of the DG in the Tau^{VLW} group, compared to the control animals. In the dorsal part, we did not find a significant change in the number of MCs between the two genotypes. These findings might be in agreement with proposed differential functionality of the dorsal and ventral parts of the DG.[131] Specifically, it has been speculated that the dorsal DG primarily contributes to cognitive functions[132], while the ventral DG is associated with stress response and emotional behaviour[133]. Furthermore, there are studies that suggest that the two areas have different input and output pathways.[131,134] Recently, it was reported that, while ventral MC project in the inner ML (agreeing with prevailing literature), dorsal MC project both in the inner and the middle ML.[134] This is a very interesting finding that suggests that ventral and dorsal MC differentially activate DGCs. In addition, variations in the expression of certain genes between ventral and dorsal DG have been reported by different groups.[131] Since Tau^{VLW} mice display depressive symptoms[35] and human patients of FTD also show alterations in their behaviour[1,2], a possible suggestion is that alterations in the ventral DG are related to behavioural symptoms. Moreover, our group recently studied new-born DGCs in Tau^{VLW} mice, and showed a decrease in branching in these cells, in the length of their primary apical dendrite,

in the number of their post-synaptic densities, in their innervation from excitatory GC and MC and an increase in their innervation from inhibitory interneurons.[37] These findings indicate that the afferent connections to new-born DGCs are impaired in the FTD mouse model. Those data are in agreement with our current findings, since one of the main afferent connections of DGCs derive from MCs. Therefore, a reduction in the number of MCs could mean a reduction in the excitatory innervation of DGCs. [135]

Another interesting finding of this study was the expression of CR in MCs of the dorsal DG. According to most studies, CR is expressed only by ventral MCs in the mouse DG.[111–113] What we saw was a gradient of CR^+ MCs, with CR expression decreasing while moving from the most lateral parts of the mouse brain, towards the midline. This gradient was observed in both Tau^{VLW} and control mice, and did not differ between genotypes. When we grouped the two most lateral, two middle and two most medial slices for each mouse, we saw a statistically significant decrease in the ratio of $Dysbindin^+$ cells that also expressed CR. We suggest that the putative lack of CR immunoreactivity in the dorsal MC of the mouse DG reported in other studies might be due to the use of coronal brain slices in most studies. As shown in the Allen Brain Atlas image, in coronal slices, the structure of the dorsal DG is more prominent closer to the midline. The expression of CR by ventral MCs persisted throughout the whole latero-medial axis. These findings further support the hypothesis that different areas of the DG could have different roles, and refocuses our attention not only on the dorso-ventral differences but also on the latero-medial ones.

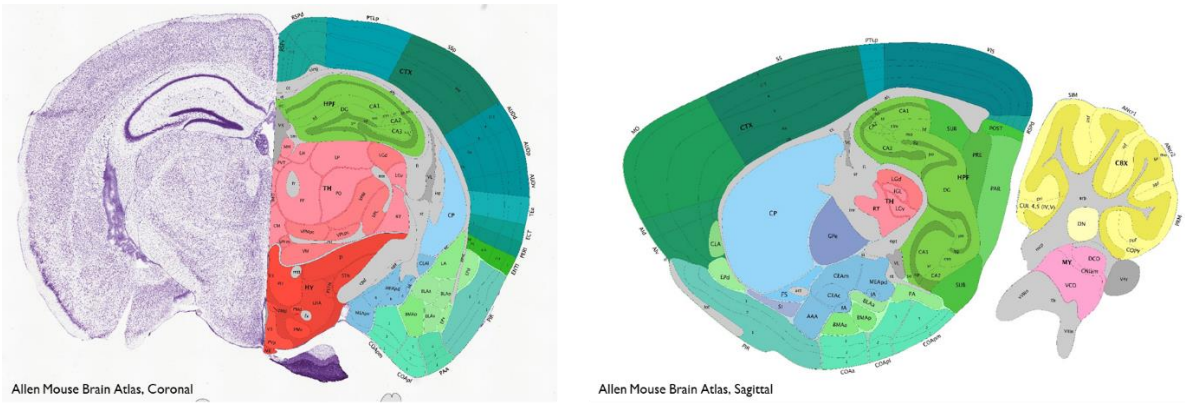

Figure 22: Allen Mouse Brain Atlas. Left: Picture of a coronal slice where the dorsal part of the DG is more prominent in the positions closer to the midline. Right: Picture of a sagittal slice of the mouse DG (most lateral points) where the dorsal part is easily distinguishable. Pictures obtained from Allen Institute.[135]

We quantified the number of CR^+ cells in patients of FTD as well as healthy control subjects. We observed several types of CR^+ cells in the human DG and the hilus. Some of them fit the MC characteristics, which were the localization in the hilus, the big size of the soma and the existence of prominent dendritic arborizations. Using these criteria, we differentiated between CR^+ MCs, CR^+ hilar interneurons, and CR^+ immature DGCs (*Table 3*). It should be noted that the latter were exclusively located at the SGZ. We found no significant differences in the cell density of CR^+ MCs between the FTD and the control group. However, we found statistically significant decreases in the density of CR^+

immature DGCs and CR^+ interneurons. These findings are in agreement with the previously reported results of decreased numbers of proliferative neuroblasts and impaired DGC differentiation in FTD patients.[128] Furthermore, it has been reported that DGCs of FTD patients show increased proximal and reduced distal dendritic branching, decreased total dendritic length and length of the primary apical dendrite, as well as increase in the inhibitory innervation.[37] In this context, the decreased density of CR^+ interneurons found might indicate that other inhibitory interneuron populations are increased in FTD brains, or that the remaining CR^+ interneurons strengthen their projections onto immature DGCs. Further investigation of different GABAergic interneuron groups is required to understand the inhibitory network of the DG and the way it is affected in FTD.

According to the few studies concerning MC marker expression in human brains, MCs of the human DG do not express CR.[114,123] Since we did find some CR^+ cells that fit our characterization criteria for MCs, we decided to perform qualitative determinations on human tissue to confirm these results. We used various established MC markers in double IHC with CR to assess co-expression. Indeed, when we labelled for Dysbindin, CART and D2R, what we saw was a big number of hilar cells that expressed the markers of interest and fit all the MC criteria that were mentioned previously Our findings could suggest that, in the human DG, distinct subpopulations of MCs exist, that express different molecular markers. Whether these MC populations expressing different markers also vary in their function is yet to be investigated. Nevertheless, we report that a subpopulation of MC does express CR, contrary to what has been reported until now.[114,123] The lack of CR expression in these studies may be due to the small number of MCs that express this marker or to the classification of those cells are hilar interneurons.

Hilar MCs are a major cell population of the DG since they are one of the two glutamatergic types of neurons in this area, along with DGCs. They both excite and indirectly inhibit GC by activating GABAergic interneurons, but their net effect on GC is not yet deciphered. A big question about MCs is their role in TLE, and as patients with AD and FTD are at higher risk of having epilepsy,[136,137] the role of these cells in neurodegenerative dementias is extremely important As mentioned earlier, MCs are significantly affected in TLE and it is not certain if their loss is the cause of the disorder, or a result of another disrupted molecular pathway. Also, the role of the surviving MCs in TLE is still largely debated. Two recent studies reported opposite results regarding the function of MCs in seizure activity. In the first study, they showed that activation of the remaining MC during the chronic phase of TLE brought a reduction of the seizure duration and inhibition of MCs at the onset of seizures developed more severe seizures, supporting that surviving MCs generally inhibit GC in TLE and thus, activating MCs can halt the spread of seizures.[138] On the other hand, the second group showed that inhibition of MCs reduced SE onset, seizure frequency and duration, thus supporting that MCs generally contribute to the hyperexcitability of GCs.[139] The differences between the two studies are mainly the phase of the seizures (chronic phase of TLE and SE) and the investigation of the surviving MCs and the whole population of

MCs. Nevertheless, it is obvious that further investigation is absolutely needed to better elucidate both the physiological function of MCs as well as their impairment in TLE.

Apart from TLE, MCs have been implicated in different pathologies, including SCZ and AD. A possible mechanism through which MCs could be involved in both these conditions is AHN. This hypothesis has a strong base, since we know that MCs provide the first excitatory input to new-born neurons of the DG and are involved in the synaptic integration of those cells in the hippocampus network and in the regulation of the NSC pool.[87–90] It has been demonstrated that in sdy mice (model of SCZ) new-born GCs have delayed maturation that could be caused by the extensive loss of MCs in those mice.[106] In AD, impaired AHN has also been demonstrated both in mouse models and in human patients.[86,140] Since MCs are involved in this process, dysfunction of these cells could contribute to the impairment of AHN, but further investigation is needed to answer this question. Apart from their involvement in AHN, MCs are related to AD through different mechanisms like increased excitability, disruption in AD-related signaling pathways and dysfunction of the MC-HIPP cell synapse.[107–110]

All in all, our results show that MCs are vulnerable to neurodegenerative diseases such as FTD. Further research in mouse models and patients with different disorders is required to elucidate the role of MCs. Of extreme importance is the need to establish robust and specific cell markers, as well as new techniques to selectively manipulate MCs, with a view to uncover the molecular pathways that these cells are involved in both in physiological and pathological conditions.

Conclusions

1) Both the dorsal and the ventral part of the DG show a decrease of their volume in a mouse model of FTDP-17, compared to control animals.
2) Hilar MCs are decreased in the ventral DG of Tau^{VLW} mice.
3) CR expression in dorsal MCs follows a gradient along the latero-medial axis of the hippocampus, with MCs losing CR expression in areas closer to the midline.
4) The density of CR^+ hilar MCs remains unchanged in FTD patients compared to and neurologically healthy control subjects.
5) The density of CR^+ immature DGCs and hilar interneurons is significantly decreased in FTD patients compared to neurologically healthy control subjects.
6) The majority (if not all) of MCs of the human DG express Dysbindin-1C, while only certain MC subpopulations might express CR, CART and D2R.

Future Directions

This project opens new avenues for future research on neurodegenerative diseases. First, it would be intriguing to explore the connectivity between MCs and new-born DGCs, especially in pathological contexts like AD or FTD. This could reveal mechanisms underlying new-born DGCs maturation and

synaptic integration and point to potential targets for treatment. Additionally, it would be interesting to perform a morphological analysis of MCs in mouse models of AD and FTD to unravel putative changes in the dendritic tree, since these cells have very extensive dendritic arborizations. The advance of optogenetic and chemo-genetic techniques might render the selective manipulation of MCs possible in the future.

Furthermore, it would be fascinating to explore the existence of distinct MC subpopulations in the human DG and the putative differences in patients with FTD and other neurodegenerative conditions.

Statistics Annex

Table 4: Results of unpaired t-tests for the comparison of the volume of the DG between C57 and Tau^{VLW} mice.

Mouse DG Volume Estimation Experiments	
Total Volume - Unpaired t-test	
TauVLW vs. C57	
P value	<0.0001
P value Summary	****
t	5.606
df	22
Mean of C57	0.55
Mean of TauVLW	0.4217
SEM	0.02289
Dorsal Volume - Unpaired t-test	
TauVLW vs. C57	
P value	<0.0001
P value Summary	****
t	5.549
df	22
Mean of C57	0.4475
Mean of TauVLW	0.3392
SEM	0.01952
Ventral Volume - Unpaired t-test	
TauVLW vs. C57	
P value	0.0466
P value Summary	*
t	2.108
df	22
Mean of C57	0.1008
Mean of TauVLW	0.0800
SEM	0.009883

Table 5: Results of 2way ANOVA for the comparison of different cell types densities between genotypes and areas of the DG.

Mouse IHC experiments					
CR+ MCs - 2way ANOVA					
Source of Variation	% of total variation	P value	P value summary		
Interaction	1.419	0.485	ns		
Area	10.72	0.063	ns		
Genotype	20.12	0.013	*		
Difference between column means					
Mean of C57	15348				
Mean of TauVLW	8148				
SE of difference	2697				
Difference between row means					
Mean of Dorsal	9.121				
Mean of Ventral	14375				
SE of difference	2697				
Multiple comparisons					
	Mean 1	Mean 2	SE of diff.	Individual P Value	Summary
Dorsal:C57 vs. Dorsal:TauVLW	11765	6476	3814	0.178	ns
Ventral:C57 vs. Ventral:TauVLW	18931	9819	3814	0.025	*
Dorsal:C57 vs. Ventral:C57	11765	18931	3814	0.072	ns
Dorsal:TauVLW vs. Ventral:TauVLW	6.476	9819	3814	0.389	ns
Dysbindin+ MCs - 2way ANOVA					
Source of Variation	% of total variation	P value	P value summary		
Interaction	0.5147	0.682	ns		
Area	1.714	0.457	ns		
Genotype	25.74	0.007	**		
Difference between column means					
Mean of C57	17131				
Mean of TauVLW	9367				
SE of difference	2651				
Difference between row means					
Mean of Dorsal	12.247				
Mean of Ventral	14250				
SE of difference	2651				
Multiple comparisons					
	Mean 1	Mean 2	SE of diff.	Individual P Value	Summary
Dorsal:C57 vs. Dorsal:TauVLW	15580	8914	3749	0.088	ns
Ventral:C57 vs. Ventral:TauVLW	18681	9819	3749	0.027	*
Dorsal:C57 vs. Ventral:C57	15580	18681	3749	0.416	ns
Dorsal:TauVLW vs. Ventral:TauVLW	8.914	9819	3749	0.811	ns

Double labelled (CR+/Dysbindin+) MCs - 2way ANOVA					
Source of Variation	% of total variation	P value	P value summary		
Interaction	1.459	0.479	ns		
Area	11.30	0.057	ns		
Genotype	19.56	0.015	*		
Difference between column means					
Mean of C57	15074				
Mean of TauVLW	8091				
SE of difference	2651				
Difference between row means					
Mean of Dorsal	8.929				
Mean of Ventral	14236				
SE of difference	2651				
Multiple comparisons					
	Mean 1	Mean 2	SE of diff.	Individual P Value	Summary
Dorsal:C57 vs. Dorsal:TauVLW	11467	6391	3750	0.188	ns
Ventral:C57 vs. Ventral:TauVLW	18681	9791	3750	0.026	*
Dorsal:C57 vs. Ventral:C57	11467	18681	3750	0.066	ns
Dorsal:TauVLW vs. Ventral:TauVLW	6.391	9791	3750	0.374	ns
CR+ Interneurons - 2way ANOVA					
Source of Variation	% of total variation	P value	P value summary		
Interaction	1.841	0.453	ns		
Area	19.11	0.022	*		
Genotype	10.15	0.087	ns		
Difference between column means					
Mean of C57	1591				
Mean of TauVLW	972.8				
SE of difference	344.8				
Difference between row means					
Mean of Dorsal	1706				
Mean of Ventral	857.8				
SE of difference	344.8				
Multiple comparisons					
	Mean 1	Mean 2	SE of diff.	Individual P Value	Summary
Dorsal:C57 vs. Dorsal:TauVLW	1883	1528	468.5	0.457	ns
Ventral:C57 vs. Ventral:TauVLW	1299	417	506.1	0.096	ns
Dorsal:C57 vs. Ventral:C57	1883	1299	487.7	0.243	ns
Dorsal:TauVLW vs. Ventral:TauVLW	1528	417	487.7	0.033	*

Table 6: Results of 2way ANOVA for the comparison of CR expression in Dysbindin^{+} cells between genotypes and positions in the latero-medial axis.

Mouse IHC experiments					
CR gradient - 2way ANOVA					
Source of Variation	% of total variation	P value	P value summary		
Interaction	0.7298	0.6165	ns		
Position on the latero-medial axis	71.29	<0.0001	****		
Genotype	1.178	0.2165	ns		
Difference between column means					
Mean of C57	15348				
Mean of TauVLW	8148				
SE of difference	2697				
Difference between row means					
Mean of C57	0.7332				
Mean of TauVLW	0.6625				
SE of difference	0.05621				
Multiple comparisons					
	Mean 1	Mean 2	SE of diff.	Individual P Value	Summary
Lateral					
C57 vs. TauVLW	1.000	1.000	0.09735	>0.9999	ns
Middle					
C57 vs. TauVLW	0.7969	0.7208	0.09735	0.4395	ns
Medial					
C57 vs. TauVLW	0.4027	0.2667	0.09735	0.1710	ns
C57					
Lateral vs. Middle	1.000	0.7969	0.09735	0.0441	*
Lateral vs. Medial	1.000	0.4027	0.09735	<0.0001	****
Middle vs. Medial	0.7969	0.4027	0.09735	0.0003	***
TauVLW					
Lateral vs. Middle	1.000	0.7208	0.09735	0.0069	**
Lateral vs. Medial	1.000	0.2667	0.09735	<0.0001	****
Middle vs. Medial	0.7208	0.2667	0.09735	<0.0001	****

Table 7: Results of unpaired t-tests for the comparison of densities of different CR+ cell types between neurologically healthy human subjects and FTD patients.

Human IHC Experiments	
CR+ MC Density - Unpaired t-test	
FTD vs Control	
P value	0.8913
P value Summary	ns
t	0.1389
df	16
Mean of Control	1158
Mean of FTD	1192
SEM	242.0
CR+ Immature neurons - Unpaired t-test	
FTD vs Control	
P value	0.0043
P value Summary	**
t	3.354
df	15
Mean of Control	2451
Mean of FTD	779.3
SEM	498.5
CR+ Interneurons - Unpaired t-test	
FTD vs Control	
P value	0.0370
P value Summary	*
t	2.276
df	16
Mean of Control	4064
Mean of FTD	2497
SEM	688.5

References

1. Erkkinen, M. G., Kim, M. O. & Geschwind, M. D. Clinical Neurology and Epidemiology of the Major Neurodegenerative Diseases. *Cold Spring Harb Perspect Biol* **10**, (2018).

2. Bang, J., Spina, S. & Miller, B. L. Non-Alzheimer's dementia 1: Frontotemporal dementia. *Lancet* **386**, 1672 (2015).

3. Le Ber, I. *et al.* Demographic, neurological and behavioural characteristics and brain perfusion SPECT in frontal variant of frontotemporal dementia. *Brain* **129**, 3051–3065 (2006).

4. Vieira, R. T. *et al.* Epidemiology of early-onset dementia: a review of the literature. *Clin Pract Epidemiol Ment Health* **9**, 88 (2013).

5. Onyike, C. U. & Diehl-Schmid, J. The Epidemiology of Frontotemporal Dementia. *Int Rev Psychiatry* **25**, 130 (2013).

6. Knopman, D. S. & Roberts, R. O. Estimating the Number of Persons with Frontotemporal Lobar Degeneration in the US Population. *J Mol Neurosci* **45**, 330 (2011).

7. Hodges, J. R., Davies, R., Xuereb, J., Kril, J. & Halliday, G. Survival in frontotemporal dementia. *Neurology* **61**, 349–354 (2003).

8. Lambert, M. A. *et al.* Estimating the burden of early onset dementia; systematic review of disease prevalence. *Eur J Neurol* **21**, 563–569 (2014).

9. Younes, K. & Miller, B. L. Frontotemporal Dementia: Neuropathology, Genetics, Neuroimaging, and Treatments. *Psychiatric Clinics of North America* **43**, 331–344 (2020).

10. Kril, J. J. & Halliday, G. M. Pathological staging of frontotemporal lobar degeneration. *J Mol Neurosci* **45**, 379–383 (2011).

11. Cairns, N. J. *et al.* Neuropathologic diagnostic and nosologic criteria for frontotemporal lobar degeneration: consensus of the Consortium for Frontotemporal Lobar Degeneration. *Acta Neuropathol* **114**, 5 (2007).

12. Seeley, W. W. *et al.* Frontal paralimbic network atrophy in very mild behavioral variant frontotemporal dementia. *Arch Neurol* **65**, 249–255 (2008).

13. Sieben, A. *et al.* The genetics and neuropathology of frontotemporal lobar degeneration. *Acta Neuropathol* **124**, 353–372 (2012).

14. Snowden, J., Neary, D. & Mann, D. Frontotemporal lobar degeneration: clinical and pathological relationships. *Acta Neuropathol* **114**, 31–38 (2007).

15. Rohrer, J. D. *et al.* Clinical and neuroanatomical signatures of tissue pathology in frontotemporal lobar degeneration. *Brain* **134**, 2565–2581 (2011).

16. MacKenzie, I. R. A. *et al.* Nomenclature and nosology for neuropathologic subtypes of frontotemporal lobar degeneration: an update. *Acta Neuropathol* **119**, 1–4 (2010).

17. Seelaar, H., Rohrer, J. D., Pijnenburg, Y. A. L., Fox, N. C. & Van Swieten, J. C. Clinical, genetic and pathological heterogeneity of frontotemporal dementia: a review. *J Neurol Neurosurg Psychiatry* **82**, 476–486 (2011).

18. Rohrer, J. D. & Warren, J. D. Phenotypic signatures of genetic frontotemporal dementia. *Curr Opin Neurol* **24**, 542–549 (2011).

19. Goldman, J. S. *et al.* Comparison of family histories in FTLD subtypes and related tauopathies. *Neurology* **65**, 1817–1819 (2005).

20. Boeve, B. F. & Hutton, M. Refining FTDP-17: Introducing FTDP-17(MAPT) and FTDP-17(PGRN). *Arch Neurol* **65**, 460 (2008).

21. Goedert, M. & Spillantini, M. G. Tau mutations in frontotemporal dementia FTDP-17 and their relevance for Alzheimer's disease. *Biochimica et Biophysica Acta (BBA) - Molecular Basis of Disease* **1502**, 110–121 (2000).

22. Goedert, M., Spillantini, M. G., Jakes, R., Rutherford, D. & Crowther, R. A. Multiple isoforms of human microtubule-associated protein tau: sequences and localization in neurofibrillary tangles of Alzheimer's disease. *Neuron* **3**, 519–526 (1989).

23. Ghetti, B. *et al.* Invited review: Frontotemporal dementia caused by microtubule-associated protein tau gene (MAPT) mutations: a chameleon for neuropathology and neuroimaging. *Neuropathol Appl Neurobiol* **41**, 24–46 (2015).

24. Guo, T., Noble, W. & Hanger, D. P. Roles of tau protein in health and disease. *Acta Neuropathol* **133**, 665–704 (2017).

25. Wszolek, Z. K. *et al.* Frontotemporal dementia and parkinsonism linked to chromosome 17 (FTDP-17). *Orphanet J Rare Dis* **1**, 30 (2006).

26. Khan, B. K. *et al.* Schizophrenia or neurodegenerative disease prodrome? Outcome of a first psychotic episode in a 35-year-old woman. *Psychosomatics* **53**, 280–284 (2012).

27. Hasegawa, M., Smith, M. J. & Goedert, M. Tau proteins with FTDP-17 mutations have a reduced ability to promote microtubule assembly. *FEBS Lett* **437**, 207–210 (1998).

28. Dayanandan, R. *et al.* Mutations in tau reduce its microtubule binding properties in intact cells and affect its phosphorylation. *FEBS Lett* **446**, 228–232 (1999).

29. Hutton, M. *et al.* Association of missense and 5'-splice-site mutations in tau with the inherited dementia FTDP-17. *Nature* **393**, 702–704 (1998).

30. D'Souza, I. *et al.* Missense and silent tau gene mutations cause frontotemporal dementia with parkinsonism-chromosome 17 type, by affecting multiple alternative RNA splicing regulatory elements. *Proc Natl Acad Sci U S A* **96**, 5598–5603 (1999).

31. Hutton, M. *et al.* Association of missense and 5'-splice-site mutations in tau with the inherited dementia FTDP-17. *Nature* **393**, 702–704 (1998).

32. Delisle, M. B. *et al.* A mutation at codon 279 (N279K) in exon 10 of the Tau gene causes a tauopathy with dementia and supranuclear palsy. *Acta Neuropathol* **98**, 62–77 (1999).

33. Clark, L. N. *et al.* Pathogenic implications of mutations in the tau gene in pallido-ponto-nigral degeneration and related neurodegenerative disorders linked to chromosome 17. *Proc Natl Acad Sci U S A* **95**, 13103–13107 (1998).

34. Lim, F. *et al.* FTDP-17 mutations in tau transgenic mice provoke lysosomal abnormalities and tau filaments in forebrain. *Molecular and Cellular Neuroscience* **18**, 702–714 (2001).

35. Llorens-Martin, M., Hernandez, F. & Avila, J. Expression of frontotemporal dementia with parkinsonism associated to chromosome 17 tau induces specific degeneration of the ventral dentate gyrus and depressive-like behavior in mice. *Neuroscience* **196**, 215–227 (2011).

36. García-Cabrero, A. M. *et al.* Hyperexcitability and epileptic seizures in a model of frontotemporal dementia. *Neurobiol Dis* **58**, 200–208 (2013).

37. Terreros-Roncal, J. *et al.* Activity-Dependent Reconnection of Adult-Born Dentate Granule Cells in a Mouse Model of Frontotemporal Dementia. *The Journal of Neuroscience* **39**, 5794 (2019).

38. Cheng, S. T. *et al.* Mental and physical activities delay cognitive decline in older persons with dementia. *Am J Geriatr Psychiatry* **22**, 63–74 (2014).

39. Merrilees, J. A model for management of behavioral symptoms in frontotemporal lobar degeneration. *Alzheimer Dis Assoc Disord* **21**, (2007).

40. Lebert, F., Stekke, W., Hasenbroekx, C. & Pasquier, F. Frontotemporal dementia: a randomised, controlled trial with trazodone. *Dement Geriatr Cogn Disord* **17**, 355–359 (2004).

41. Herrmann, N. *et al.* Serotonergic function and treatment of behavioral and psychological symptoms of frontotemporal dementia. *Am J Geriatr Psychiatry* **20**, 789–797 (2012).

42. Prodan, C. I., Monnot, M. & Ross, E. D. Behavioural abnormalities associated with rapid deterioration of language functions in semantic dementia respond to sertraline. *J Neurol Neurosurg Psychiatry* **80**, 1416–1417 (2009).

43. Moretti, R., Torre, P., Antonello, R. M., Cazzato, G. & Bava, A. Frontotemporal dementia: paroxetine as a possible treatment of behavior symptoms. A randomized, controlled, open 14-month study. *Eur Neurol* **49**, 13–19 (2003).

44. Swartz, J. R., Miller, B. L. & Darby, A. L. Frontotemporal Dementia: Treatment Response to Serotonin Selective Reuptake Inhibitors. *J Clin Psychiatry* **58**, 7480 (1997).

45. Sanchez, C., Reines, E. H. & Montgomery, S. A. A comparative review of escitalopram, paroxetine, and sertraline: Are they all alike? *Int Clin Psychopharmacol* **29**, 185–196 (2014).

46. Reed, D. A., Johnson, N. A., Thompson, C., Weintraub, S. & Mesulam, M. M. A clinical trial of bromocriptine for treatment of primary progressive aphasia. *Ann Neurol* **56**, 750 (2004).

47. Huey, E. D., Garcia, C., Wassermann, E. M., Tierney, M. C. & Grafman, J. Stimulant Treatment of Frontotemporal Dementia in 8 Patients. *J Clin Psychiatry* **69**, 1981 (2008).

48. Rahman, S. *et al.* Methylphenidate ('Ritalin') can ameliorate abnormal risk-taking behavior in the frontal variant of frontotemporal dementia. *Neuropsychopharmacology* **31**, 651–658 (2006).

49. Ondo, W. G. Tetrabenazine treatment for stereotypies and tics associated with dementia. *J Neuropsychiatry Clin Neurosci* **24**, 208–214 (2012).

50. Tsai, R. M. & Boxer, A. L. Treatment of Frontotemporal Dementia. *Curr Treat Options Neurol* **16**, 319 (2014).

51. Ljubenkov, P. A. *et al.* Effect of the Histone Deacetylase Inhibitor FRM-0334 on Progranulin Levels in Patients With Progranulin Gene Haploinsufficiency: A Randomized Clinical Trial. *JAMA Netw Open* **4**, (2021).

52. Yanamandra, K. *et al.* Anti-tau antibodies that block tau aggregate seeding in vitro markedly decrease pathology and improve cognition in vivo. *Neuron* **80**, 402 (2013).

53. Boxer, A. L. *et al.* The advantages of frontotemporal degeneration drug development (part 2 of frontotemporal degeneration: the next therapeutic frontier). *Alzheimers Dement* **9**, 189–198 (2013).

54. Amaral, D. G., Scharfman, H. E. & Lavenex, P. The dentate gyrus: fundamental neuroanatomical organization (dentate gyrus for dummies). *Prog Brain Res* **163**, 3 (2007).

55. Insausti, R. & Amaral, D. G. Hippocampal Formation. *The Human Nervous System: Second Edition* 871–914 (2003) doi:10.1016/B978-012547626-3/50024-7.

56. Lopez-Rojas, J. & Kreutz, M. R. Mature granule cells of the dentate gyrus--Passive bystanders or principal performers in hippocampal function? *Neurosci Biobehav Rev* **64**, 167–174 (2016).

57. Morgan, R. J., Santhakumar, V. & Soltesz, I. Modeling the dentate gyrus. *Prog Brain Res* **163**, 639–658 (2007).

58. Jiao, Y. & Nadler, J. V. Stereological analysis of GluR2-immunoreactive hilar neurons in the pilocarpine model of temporal lobe epilepsy: correlation of cell loss with mossy fiber sprouting. *Exp Neurol* **205**, 569–582 (2007).

59. Scharfman, H. E. & Myers, C. E. Hilar mossy cells of the dentate gyrus: a historical perspective. *Front Neural Circuits* **6**, (2013).

60. Scharfman, H. E. The enigmatic mossy cell of the dentate gyrus. *Nature Reviews Neuroscience* vol. 17 562–575 Preprint at https://doi.org/10.1038/nrn.2016.87 (2016).

61. Henze, D. A., Urban, N. N. & Barrionuevo, G. *THE MULTIFARIOUS HIPPOCAMPAL MOSSY FIBER PATHWAY: A REVIEW*. www.elsevier.com/locate/neuroscience.

62. Buckmaster, P., Wenzel, H., Kunkel, D. & Schwartzkroin, P. Axon arbors and synaptic connections of hippocampal mossy cells in the rat in vivo. *Journal of Comparative Neurology* (1996) doi:10.1002/(SICI)1096-9861(19960304)366:2.

63. Ribak, C. E., Seress, L. & Amaral, D. G. The development, ultrastructure and synaptic connections of the mossy cells of the dentate gyrus. *J Neurocytol* **14**, 835–857 (1985).

64. Buckmaster, P. S., Strowbridge, B. W., Kunkel, D. D., Schmiege, D. L. & Schwartzkroin, P. A. Mossy cell axonal projections to the dentate gyrus molecular layer in the rat hippocampal slice. *Hippocampus* **2**, 349–362 (1992).

65. Leranth, C., Szeidemann, Z., Hsu, M. & Buzsáki, G. AMPA receptors in the rat and primate hippocampus: a possible absence of GluR2/3 subunits in most interneurons. *Neuroscience* **70**, 631–652 (1996).

66. Soriano, E. & Frotscher, M. Mossy cells of the rat fascia dentata are glutamate-immunoreactive. *Hippocampus* **4**, 65–69 (1994).

67. Scharfman, H. E. Electrophysiological evidence that dentate hilar mossy cells are excitatory and innervate both granule cells and interneurons. *J Neurophysiol* **74**, 179–194 (1995).

68. Larimer, P. & Strowbridge, B. W. Nonrandom local circuits in the dentate gyrus. *J Neurosci* **28**, 12212–12223 (2008).

69. Ratzliff, A. D. H., Howard, A. L., Santhakumar, V., Osapay, I. & Soltesz, I. Rapid Deletion of Mossy Cells Does Not Result in a Hyperexcitable Dentate Gyrus: Implications for Epileptogenesis. *Journal of Neuroscience* **24**, 2259–2269 (2004).

70. Scharfman, H. E. Differentiation of rat dentate neurons by morphology and electrophysiology in hippocampal slices: granule cells, spiny hilar cells and aspiny 'fast-spiking' cells. *Epilepsy Res Suppl* **7**, 93 (1992).

71. Scharfman, H. E. Characteristics of spontaneous and evoked EPSPs recorded from dentate spiny hilar cells in rat hippocampal slices. *J Neurophysiol* **70**, 742–757 (1993).

72. Scharfman, H. E. & Schwartzkroin, P. A. Electrophysiology of morphologically identified mossy cells of the dentate hilus recorded in guinea pig hippocampal slices. *J Neurosci* **8**, 3812–3821 (1988).

73. Duffy, A. M., Schaner, M. J., Chin, J. & Scharfman, H. E. Expression of c-fos in hilar mossy cells of the dentate gyrus in vivo. *Hippocampus* **23**, 649–655 (2013).

74. Lysetskiy, M., Földy, C. & Soltesz, I. Long- and short-term plasticity at mossy fiber synapses on mossy cells in the rat dentate gyrus. *Hippocampus* **15**, 691–696 (2005).

75. Hashimotodani, Y. *et al.* LTP at Hilar Mossy Cell-Dentate Granule Cell Synapses Modulates Dentate Gyrus Output by Increasing Excitation/Inhibition Balance. *Neuron* **95**, 928-943.e3 (2017).

76. Kleschevnikov, A. M. & Routtenberg, A. Long-term potentiation recruits a trisynaptic excitatory associative network within the mouse dentate gyrus. *European Journal of Neuroscience* **17**, 2690–2702 (2003).

77. Hetherington, P. A., Austin, K. B. & Shapiro, M. L. Ipsilateral associational pathway in the dentate gyrus: An excitatory feedback system that supports N-methyl-D-aspartate—dependent long-term potentiation. *Hippocampus* **4**, 422–438 (1994).

78. Cayco-Gajic, N. A. & Silver, R. A. Re-evaluating Circuit Mechanisms Underlying Pattern Separation. *Neuron* **101**, 584–602 (2019).

79. Sahay, A., Wilson, D. A. & Hen, R. Pattern separation: a common function for new neurons in hippocampus and olfactory bulb. *Neuron* **70**, 582 (2011).

80. Leutgeb, J. K., Leutgeb, S., Moser, M. B. & Moser, E. I. Pattern separation in the dentate gyrus and CA3 of the hippocampus. *Science (1979)* **315**, 961–966 (2007).

81. Knierim, J. J. & Neunuebel, J. P. Tracking the flow of hippocampal computation: Pattern separation, pattern completion, and attractor dynamics. (2015) doi:10.1016/j.nlm.2015.10.008.

82. GoodSmith, D. *et al.* Spatial Representations of Granule Cells and Mossy Cells of the Dentate Gyrus. *Neuron* **93**, 677-690.e5 (2017).

83. Danielson, N. B. *et al.* In Vivo Imaging of Dentate Gyrus Mossy Cells in Behaving Mice. *Neuron* **93**, 552-559.e4 (2017).

84. Eriksson, P. S. *et al.* Neurogenesis in the adult human hippocampus. *Nat Med* **4**, 1313–1317 (1998).

85. Altman, J. Autoradiographic investigation of cell proliferation in the brains of rats and cats. *Anat Rec* **145**, 573–591 (1963).

86. Moreno-Jiménez, E. P. *et al.* Adult hippocampal neurogenesis is abundant in neurologically healthy subjects and drops sharply in patients with Alzheimer's disease. *Nat Med* **25**, 554–560 (2019).

87. Chancey, J. H., Poulsen, D. J., Wadiche, J. I. & Overstreet-Wadiche, L. Hilar Mossy Cells Provide the First Glutamatergic Synapses to Adult-Born Dentate Granule Cells. *Journal of Neuroscience* **34**, 2349–2354 (2014).

88. Yeh, C. Y. *et al.* Mossy Cells Control Adult Neural Stem Cell Quiescence and Maintenance through a Dynamic Balance between Direct and Indirect Pathways. *Neuron* **99**, 493-510.e4 (2018).

89. Gonzalez-Reyes, L. E. *et al.* Sonic Hedgehog is expressed by hilar mossy cells and regulates cellular survival and neurogenesis in the adult hippocampus. doi:10.1038/s41598-019-53192-4.

90. Noguchi, H., Arela, J. C., Ngo, T. T., Cocas, L. & Pleasure, S. J. Shh from mossy cells contributes to preventing NSC pool depletion after seizure-induced neurogenesis and in aging. *bioRxiv* (2023) doi:10.1101/2023.08.21.554173.

91. Blümcke, I. *et al.* Loss of hilar mossy cells in Ammon's horn sclerosis. *Epilepsia* **41**, (2000).

92. Kecskés, A., Czéh, B. & Kecskés, M. Mossy cells of the dentate gyrus: Drivers or inhibitors of epileptic seizures? *Biochimica et Biophysica Acta - Molecular Cell Research* vol. 1869 Preprint at https://doi.org/10.1016/j.bbamcr.2022.119279 (2022).

93. Schwartzkroin, P. A. *et al.* Possible mechanisms of seizure-related cell damage in the dentate hilus. *Epilepsy Res Suppl* **12**, 317–324 (1996).

94. Sloviter, R. S. Calcium-binding protein (calbindin-D28k) and parvalbumin immunocytochemistry: Localization in the rat hippocampus with specific reference to the selective vulnerability of hippocampal neurons to seizure activity. *Journal of Comparative Neurology* **280**, 183–196 (1989).

95. Yuan, Y., Wang, H., Wei, Z. & Li, W. Impaired Autophagy in Hilar Mossy Cells of the Dentate Gyrus and Its Implication in Schizophrenia. *Journal of Genetics and Genomics* **42**, 1–8 (2015).

96. Sloviter, R. S. Permanently altered hippocampal structure, excitability, and inhibition after experimental status epilepticus in the rat: The "dormant basket cell" hypothesis and its possible relevance to temporal lobe epilepsy. *Hippocampus* **1**, 41–66 (1991).

97. Mitchell, J., Gatherer, M. & Sundstrom, L. E. Loss of hilar somatostatin neurons following tetanus toxin-induced seizures. *Acta Neuropathol* **89**, 425–430 (1995).

98. Mitchell, J., Cook, I. & Hervey, V. Effect of seizures on hippocampal peptidergic neurons. *Neuropathol Appl Neurobiol* **23**, 299–306 (1997).

99. Santhakumar, V. *et al.* Granule cell hyperexcitability in the early post-traumatic rat dentate gyrus: The 'irritable mossy cell' hypothesis. *Journal of Physiology* **524**, 117–134 (2000).

100. Santhakumar, V., Aradi, I. & Soltesz, I. Role of mossy fiber sprouting and mossy cell loss in hyperexcitability: A network model of the dentate gyrus incorporating cell types and axonal topography. *J Neurophysiol* **93**, 437–453 (2005).

101. Scharfman, H. E., Smith, K. L., Goodman, J. H. & Sollas, A. L. Survival of dentate hilar mossy cells after pilocarpine-induced seizures and their synchronized burst discharges with area CA3 pyramidal cells. *Neuroscience* **104**, 741–759 (2001).

102. Owen, M. J., Sawa, A. & Mortensen, P. B. Schizophrenia. *The Lancet* **388**, 86–97 (2016).

103. Ayalew, M. *et al.* Convergent functional genomics of schizophrenia: from comprehensive understanding to genetic risk prediction. *Molecular Psychiatry 2012 17:9* **17**, 887–905 (2012).

104. Straub, R. E. *et al.* Genetic Variation in the 6p22.3 Gene DTNBP1, the Human Ortholog of the Mouse Dysbindin Gene, Is Associated with Schizophrenia. *Am. J. Hum. Genet* **71**, 337–348 (2002).

105. Talbot, K. *et al.* Synaptic Dysbindin-1 Reductions in Schizophrenia Occur in an Isoform-Specific Manner Indicating Their Subsynaptic Location. *PLoS One* **6**, e16886 (2011).

106. Wang, H. *et al.* Dysbindin-1C Is Required for the Survival of Hilar Mossy Cells and the Maturation of Adult Newborn Neurons in Dentate Gyrus. *Journal of Biological Chemistry* **289**, 29060–29072 (2014).

107. Kazim, S. F. *et al.* Early-onset network hyperexcitability in presymptomatic Alzheimer's disease transgenic mice is suppressed by passive immunization with anti-human APP/Aβ antibody and by mGluR5 blockade. *Front Aging Neurosci* **9**, 251155 (2017).

108. Alcantara-Gonzalez, D. *et al.* Hippocampal mossy cells exhibit some of the earliest signs of increased excitability in the Tg2576 model of Alzheimer's disease neuropathology. *Alzheimer's & Dementia* **18**, e069163 (2022).

109. Li, S. *et al.* Alzheimer-like tau accumulation in dentate gyrus mossy cells induces spatial cognitive deficits by disrupting multiple memory-related signaling and inhibiting local neural circuit. *Aging Cell* **21**, (2022).

110. Deng, M. *et al.* Mossy cell synaptic dysfunction causes memory imprecision via miR-128 inhibition of STIM2 in Alzheimer's disease mouse model. *Aging Cell* **19**, (2020).

111. Liu, Y., Fujise, N. & Kosaka, T. Distribution of calretinin immunoreactivity in the mouse dentate gyrus. I. General description. *Exp Brain Res* **108**, (1996).

112. Blasco-Ibáñez, J. M. & Freund, T. F. Distribution, ultrastructure, and connectivity of calretinin-immunoreactive mossy cells of the mouse dentate gyrus. *Hippocampus* **7**, 307–320 (1997).

113. Fujise, N., Liu, Y., Hori, N. & Kosaka, T. Distribution of calretinin immunoreactivity in the mouse dentate gyrus: II. Mossy cells, with special reference to their dorsoventral difference in calretinin immunoreactivity. *Neuroscience* **82**, 181–200 (1997).

114. Seress, L., Ábrahám, H., Czéh, B., Fuchs, E. & Léránth, C. Calretinin expression in hilar mossy cells of the hippocampal dentate gyrus of nonhuman primates and humans. *Hippocampus* **18**, 425–434 (2008).

115. Gangarossa, G. *et al.* Characterization of dopamine D1 and D2 receptor-expressing neurons in the mouse hippocampus. *Hippocampus* **22**, 2199–2207 (2012).

116. Seress, L., Ábrahám, H., Dóczi, T., Lázár, G. & Kozicz, T. Cocaine- and amphetamine-regulated transcript peptide (CART) is a selective marker of rat granule cells and of human mossy cells in the hippocampal dentate gyrus. *Neuroscience* **125**, 13–24 (2004).

117. Jiao, Y. & Nadler, J. V. Stereological analysis of GluR2-immunoreactive hilar neurons in the pilocarpine model of temporal lobe epilepsy: correlation of cell loss with mossy fiber sprouting. *Exp Neurol* **205**, 569 (2007).

118. Freund, T. F., Hájos, N., Acsády, L., Görcs, T. J. & Katona, I. Mossy cells of the rat dentate gyrus are immunoreactive for calcitonin gene-related peptide (CGRP). *Eur J Neurosci* **9**, 1815–1830 (1997).

119. Chiu, C. Q. & Castillo, P. E. Input-specific plasticity at excitatory synapses mediated by endocannabinoids in the dentate gyrus. *Neuropharmacology* **54**, 68 (2008).

120. Oh, Y. S. *et al.* SMARCA3, a Chromatin-Remodeling Factor, Is Required for p11-Dependent Antidepressant Action. *Cell* **152**, 831 (2013).

121. Patel, A. & Bulloch, K. Type II glucocorticoid receptor immunoreactivity in the mossy cells of the rat and the mouse hippocampus. *Hippocampus* **13**, 59–66 (2003).

122. Choi, Y.-S. *et al.* Status Epilepticus-Induced Somatostatinergic Hilar Interneuron Degeneration Is Regulated by Striatal Enriched Protein Tyrosine Phosphatase. *The Journal of Neuroscience* **27**, 2999–3009 (2007).

123. Tóth, K. *et al.* Loss and reorganization of calretinin-containing interneurons in the epileptic human hippocampus. *Brain* **133**, 2763–2777 (2010).

124. Lavenex, P., Lavenex, P. B., Bennett, J. L. & Amaral, D. G. Postmortem changes in the neuroanatomical characteristics of the primate brain: Hippocampal formation. *Journal of Comparative Neurology* **512**, 27–51 (2009).

125. Talbot, K. *et al.* Dysbindin-1 is a synaptic and microtubular protein that binds brain snapin. *Hum Mol Genet* **15**, 3041–3054 (2006).

126. Gulfo, M. C. *et al.* Dopamine D2 receptors in mossy cells reduce excitatory transmission and are essential for hippocampal function. *bioRxiv* (2023) doi:10.1101/2023.05.05.539468.

127. Llorens-Martín, M., Torres-Alemán, I. & Trejo, J. L. Pronounced individual variation in the response to the stimulatory action of exercise on immature hippocampal neurons. *Hippocampus* **16**, 480–490 (2006).

128. Terreros-Roncal, J. *et al.* Impact of neurodegenerative diseases on human adult hippocampal neurogenesis. *Science (1979)* **374**, 1106–1113 (2021).

129. Toni, N. & Schinder, A. F. Maturation and Functional Integration of New Granule Cells into the Adult Hippocampus. *Cold Spring Harb Perspect Biol* **8**, (2016).

130. Mu, Y., Zhao, C. & Gage, F. H. Dopaminergic modulation of cortical inputs during maturation of adult-born dentate granule cells. *J Neurosci* **31**, 4113–4123 (2011).

131. Fanselow, M. S. & Dong, H. W. Are The Dorsal and Ventral Hippocampus functionally distinct structures? *Neuron* **65**, 7 (2010).

132. Van Praag, H., Christie, B. R., Sejnowski, T. J. & Gage, F. H. Running enhances neurogenesis, learning, and long-term potentiation in mice. *Proc Natl Acad Sci U S A* **96**, 13427–13431 (1999).

133. Sahay, A. & Hen, R. Adult hippocampal neurogenesis in depression. *Nat Neurosci* **10**, 1110–1115 (2007).

134. Botterill, J. J., Gerencer, K. J., Vinod, K. Y., Alcantara-Gonzalez, D. & Scharfman, H. E. Dorsal and ventral mossy cells differ in their axonal projections throughout the dentate gyrus of the mouse hippocampus. *Hippocampus* **31**, 522–539 (2021).

135. Atlas Thumbnails :: Allen Brain Atlas: Mouse Brain. https://mouse.brain-map.org/experiment/thumbnails/100048576?image_type=atlas.

136. Arnaldi, D. *et al.* Epilepsy in Neurodegenerative Dementias: A Clinical, Epidemiological, and EEG Study. *J Alzheimers Dis* **74**, 865–874 (2020).

137. Vossel, K. A., Tartaglia, M. C., Nygaard, H. B., Zeman, A. Z. & Miller, B. L. Epileptic activity in Alzheimer's disease: causes and clinical relevance. *Lancet Neurol* **16**, 311–322 (2017).

138. Bui, A. D. *et al.* Dentate gyrus mossy cells control spontaneous convulsive seizures and spatial memory. *Science (1979)* **359**, 787–790 (2018).

139. Botterill, J. J. *et al.* An Excitatory and Epileptogenic Effect of Dentate Gyrus Mossy Cells in a Mouse Model of Epilepsy. *Cell Rep* **29**, 2875-2889.e6 (2019).

140. Zhou, Y. *et al.* Mechanisms of abnormal adult hippocampal neurogenesis in Alzheimer's disease. *Front Neurosci* **17**, 1125376 (2023).